EXPERIMENTAL FEEDBACK OF FRACTIONAL ORDER STATES OF A LIGHTLY DAMPED STRUCTURE

THESIS

ROBERT C. McCALL

AFIT/GA/92M/01

DEPARTMENT OF THE AIR FORCE
AIR UNIVERSITY
AIR FORCE INSTITUTE OF TECHNOLOGY

Wright-Patterson Air Force Base, Ohio

AFIT/GA/ENY/90M-01

EXPERIMENTAL FEEDBACK OF FRACTIONAL ORDER STATES OF A LIGHTLY DAMPED STRUCTURE

THESIS

ROBERT C. McCALL

AFIT/GA/92M/01

AFIT/GA/ENY/92M-01

EXPERIMENTAL FEEDBACK OF FRACTIONAL ORDER STATES OF A LIGHTLY DAMPED STRUCTURE

Thesis

Presented to the Faculty of the School of Engineering
of the Air Force Institute of Technology
Air University
In Partial Fulfillment of the
Requirements for the Degree of
Master of Science in Astronautical Engineering

Robert C. McCall, B.S.

March 1992

Table of Contents

List of Figures

List of Tables

List of Symbols

A	state space model system matrix
B	state space model input matrix
c	reduced damping matrix
c	capacitance per unit length in the infinite analog, specific heat
C	capacitance
D[ ]	differentiation operator
D	shows the location and direction of force inputs to the structure
E	electrical potential (voltage)
E_j	electrical potential (voltage) across the j^{th} pair of resistors and capacitors in the Oldham-Zoski circuit
F[ ]	Fourier operator
$\tilde{\mathbf{F}}(t)$	Force vector in expanded equations of motion
g,G	geometric factors, governing the relationship between adjacent resistors and capacitors
G	gain matrix
$\mathbf{G_p}$	gain matrix for the integer order pole placement
G1	gain matrix for the case of where all measured states from both midpoint and tip of the beam are fed back
G2	gain matrix for the pole placement case where velocity and $D2^{\frac{3}{2}}$ measurements from both midpoint and tip of the beam are fed back
$\mathbf{G^*}$	gain matrix for the LQR case where $\underline{y}$ is composed of measurements taken solely at the midpoint of the beam
$\mathbf{G^*}$	gain matrix for the case where $\underline{y}$ is composed of velocity and $D2^{\frac{3}{2}}$ measurements taken at midpoint and tip of the beam

$i(t)$	electrical current
J	quadratic performance index
k	thermal conductivity
$\mathbf{k}$	reduced order stiffness matrix
$\mathbf{k_o}$	finite-element stiffness matrix
$\tilde{\mathbf{K}}$	pseudo-stiffness matrix
$L[\,]$	Laplace operator
$\mathbf{m}$	reduced order mass matrix
$\mathbf{M}$	finite-element stiffness matrix
$\tilde{\mathbf{M}}$	pseudo-mass matrix
$\dot{q}$	rate of heat transfer
$\mathbf{Q}$	state weighting in quadratic performance index
r	resistance per unit length in the infinite analog
R	resistance
$R(\beta)$	remainder of the synthetic division in the pole placement method
$\mathbf{R}$	control weighting in quadratic performance index
s	Laplace parameter
$\mathbf{S}$	solution to the matrix Riccati equation
T	temperature
T_s	settling time
u	force input to the system
$\mathbf{x}$	state vector of physical coordinates
$\mathbf{x}_F$	state vector of physical coordinates containing $D^{\frac{1}{2}}$ and $D^{\frac{3}{2}}$ terms in addition to positions and velocities
$\underline{y}$	mixed fractional and integer order state vector
$\mathbf{z}$	column vector of physical displacements

$\tilde{z}$	expanded column vector of physical coordinates
$Z(\beta)$	characteristic equation of the closed-loop system ir the β plane
α	order of fractional differentiation
$\alpha(s)$	desired characteristic equation of closed-loop system
β	$\sqrt{s}$
Γ	Gamma function (sometimes called the factorial function)
ζ	damping coefficient
Φ	modal transformation matrix
$\tilde{\Phi}$	modal transformation matrix for the expanded equations of motion
Φ_A	modal transformation from η to x
Φ_B	modal transformation from η to y
Φ^*	state transformation from z to y, where y is composed of measurements taken solely at the midpoint of the beam
Φ^*	state transformation from z to y, where y is composed ofvelocity and $D2^{\frac{3}{}}$ measurements taken at midpoint and tip of the beam
η	column vector of modal coordinates
ν	order of fractional differintegration
$\Psi(\beta)$	quotient of synthetic division in the pole placement method
ρ	density
ω	angular frequency
w_n	natural frequency
$\Omega(\beta)$	desired closed loop poles in the β plane

Abstract

The purpose of this study was to investigate the effectiveness of using fractional order time derivatives of position feedback signals in the active control of vibration. To that end, circuitry was built and evaluated that finds the half order derivative of an input signal. The magnitude response of the fractional derivative circuits is very good, but there are large phase shifts present that may degrade the performance of the controllers. Two methods of incorporating the fractional derivative signals into the controller were examined. One method involved developing a similarity transformation that transforms an integer order state controller into an equivalent controller using fractional or mixed fractional and integer order signals. The second method was a form of traditional pole placement techniques that allowed the direct design of a controller using fractional and integer order feedback signals. Designs were tested on an inverted cantilever beam with control provided by a shaker, and compared to theoretical predictions and to traditional integer order controllers. There is a discrepancy in the modeling that manifests itself as a large offset in magnitude, particularly at very low frequencies. However, controllers utilizing fractional order feedback provided nearly identical control authority to the traditional integer order designs.

Experimental Feedback of Fractional Order States of a Lightly Damped Structure

I. Introduction

The increasing size of current and proposed space platforms has created new problems in the control of unwanted vibrations. Because of the weight penalties on putting a platform in orbit, structures are made as light-weight as is possible. This combination of increasing size and minimal weight construction inevitably leads to problems with large amplitude, low frequency vibrations. This trend runs contrary to the increasingly stringent stability requirements needed for proposed missions. The Hubble Space Telescope experienced unwanted vibrations from thermal stresses that interfered with its mission. The proposed NASA space station needs to remain stable for docking manuevers with the shuttle. The Strategic Defense Initiative in particular requires very precise pointing maneuvers and rapid settling time after retargeting.

All of these situations have led to an increasing interest in the active control of vibration. Passive systems provide an effective means of controlling higher frequency vibration, but are of limited effectiveness in

controlling the low frequency modes with their potentially large displacements. The most likely solutions will involve whatever combination of passive and active damping most effectively fulfill specific mission requirements. This thesis will focus exclusively on the area of active control of vibration. Extensive research has taken place in this area (See especially (8) and (17) which survey research in the field), but many problems remain to be solved.

The current research effort grew out of an interest in controlling viscoelastically damped structures more precisely. Fractional derivatives of stress and strain are effective in modelling viscoelastic behavior (3-7, 28), and more amenable to an analytical treatment than an arbitrary curve-fit of a damping material's stress-strain curve. Klonoski (14) first tested direct analog feedback of fractional derivatives of position. Yang (30) developed a method of transforming traditional LQR gains to allow for the possibility of feeding back fractional derivatives of position and velocity in a mathematically optimal fashion. The main objective of this thesis is to demonstrate that Yang's work on active damping of a structure utilizing fractional derivative feedback is viable in an experimental situation. An alternative approach using pole-placement techniques (15) will be examined as well.

To that end, circuitry to obtain the required fractional derivative feedback was built and tested, the experimental structure and apparatus was modeled and verified, and control of the structure was attempted for both integer and fractional state feedback.

II. Overview of Fractional Derivatives

Fractional calculus is a little known cousin of the classical calculus, and is nearly as old. All scientists and engineers will readily recognize $\frac{d^v [f(x)]}{dt^v}$ as the derivative with respect to time of a function f(x), but very few have considered what would happen if v is not an integer. The history of fractional calculus begins in 1695 with L'Hospital asking this question of Leibnitz. Leibnitz said in his reply that it would lead to a paradox, but that "Some day it would lead to useful consequences" (23). Euler, Laplace, and Fourier all considered the problem at various times, but it was the contributions of Liouville, Abel, Heaviside and Riemann (23) that finally formalized the theory of fractional order derivatives.

A fractional derivative is a linear operator that generalizes the concept of order of differentiation from integer powers only to fractional values. The extended Riemann-Liouville fractional derivative operator is defined (2) as:

$$D^v [w(t)] = \frac{d}{dt} \int_0^t \frac{w(\tau)}{\Gamma(1-v)\,(t-\tau)^v}\, d\tau \,, \qquad 0 \le v \le 1 \tag{1}$$

where Γ is the Gamma function given by

$$\Gamma(x) = \int_0^\infty e^{-t}\, t^{x-1}\, dt \tag{2}$$

This definition is consistent with the rules that we expect of a derivative operator. It is a linear operator and the composition rule is valid (2: 8-10),

$$D^{\nu}\left[w(t) + v(t)\right] = D^{\nu}\left[w(t)\right] + D^{\nu}\left[v(t)\right] \tag{3}$$

and

$$D^{\nu}\left[D^{\mu}\left[w(t)\right]\right] = D^{\nu+\mu}\left[w(t)\right] \tag{4}$$

It is in the Laplace and Fourier transform domains that fractional derivatives are the easiest to work with. In the Laplace transform domain the fractional derivative operator with zero initial conditions has the property

$$L[D^{\nu}[x(t)]] = s^{\nu} L[x(t)] \tag{5}$$

where L is the Laplace transform operator

$$L[x(t)] = \int_0^{\infty} x(t) e^{-st} dt \tag{6}$$

Similarly, in the Fourier transform domain,

$$F[D^{\nu}[x(t)]] = (i\omega)^{\nu} F[x(t)] \tag{7}$$

where F is the Fourier transform operator

$$F[x(t)] = \int_0^\infty x(t)e^{-i\omega t}\,dt \tag{8}$$

To gain some insight into how the fractional derivative relates to the traditional derivative, consider a sinusoidal signal,

$$w(t) = \sin(\omega t) \tag{9}$$

The first-order derivative of this is simply

$$D^1[w(t)] = \omega\cos(\omega t) = \omega\sin(\omega t + \frac{\pi}{2}) \tag{10}$$

So, the derivative causes a change in magnitude ω and a phase shift ($\frac{\pi}{2}$ radians or 90°) from the initial signal. The fractional derivative, in this case the half order derivative, displays a similar behavior (asymptotically) as t approaches infinity and with zero initial conditions

$$\lim_{t\to\infty} D^{\frac{1}{2}}[w(t)] = \sqrt{\omega}\sin(\omega t + \frac{\pi}{4}) \tag{11}$$

The restriction of t approaching infinity (steady-state motion) occurs because of transients introduced with the fractional derivative. The half order derivative seems, in a certain sense, to lie "between" the signal and its first-order derivative (See Figure 1). Its phase shift is 45°, midway between the unshifted original signal and the 90° phase shift of the first-order derivative.

Its magnitude is scaled by $\sqrt{\omega}$, compared with ω for the first-order derivative. It looks as if the half-order derivative could almost be interpolated between these two signals. Heuristically this is comforting, since it demonstrates that the behavior of the fractional derivative bears some relation to the more familiar mathematics of integer order calculus. This is not a completely arbitrary example since by using a Fourier series expansion, many piecewise continuous periodic functions can be written as a sum of sinusoids.

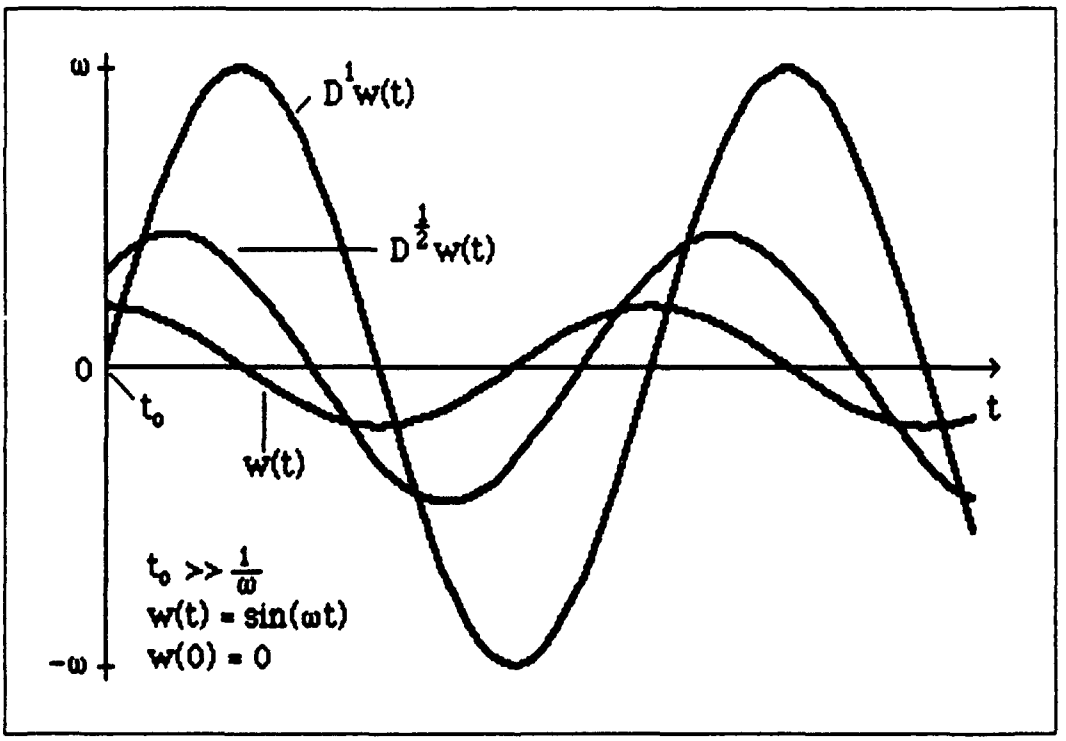

Figure 1. Comparison of Fractional And Integer Order Differentiation

III. Development of Fractional Differentiating Circuits

Overview

In order to implement the fractional calculus control scheme, it was necessary to build some type of circuit that was capable of fractional differentiation or integration. Because of problems with low-frequency drift present in integration circuits, it was decided to concentrate on building differentiators.

Two circuit designs were selected from the open literature, and both types were built and tested to see which had better performance. The *minimal criteria for success were chosen* to be a phase shift of $45° \pm 5°$, and a slope of 10 ± 0.5 dB/decade on a log-magnitude plot, within a frequency range of 1 to 100 hertz.

Since accelerometers were chosen as the sensors in this experiment, it was necessary to first integrate the acceleration signal twice to obtain position and velocity measurements of the response. Integer order integrators with good low frequency response were available from a previous experiment (9), so this was not a problem. The $D^{\frac{1}{2}}[z(t)]$ and $D^{\frac{3}{2}}[z(t)]$ signals were obtained by passing the position and velocity signals, respectively, through half-order differentiation circuits.

Oldham-Zoski Circuit

The first circuit that was examined was developed by Oldham and Zoski (21) for use in electrochemical analysis. The basic component of the circuit is the domino ladder network, which consists of interconnected chains of resistors and capacitors (See Figure 2).

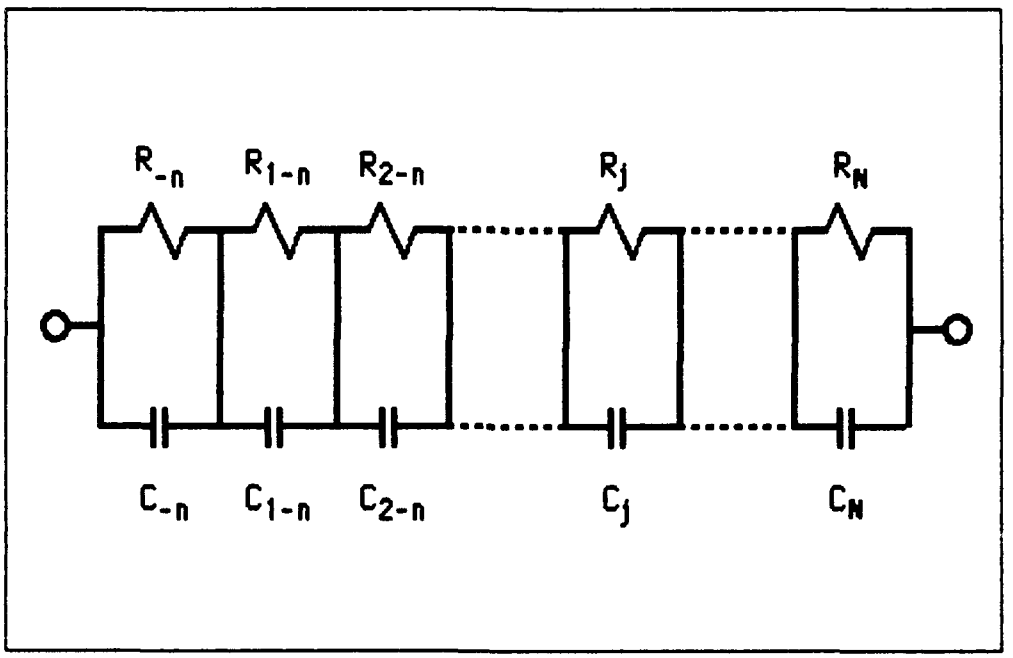

Figure 2. Domino Ladder Circuit

The magnitude of the potential, $E_j(t)$, generated across the jth pair of components, C_j and R_j, when a current, i(t), is passed through the entire network is given by

$$i(t) = \frac{E_j(t)}{R_j} + C_j \frac{d}{dt} E_j(t) \qquad (12)$$

Eq (12) may be solved to find

$$E_j(t) = \frac{1}{C_j}\int_0^t i(t-\tau)\exp\left\{\frac{-\tau}{R_jC_j}\right\}d\tau \qquad (13)$$

where τ is an variable of integration. Since the current, i, is common to all pairs of components, it follows that the potential across the entire network is

$$E_j(t) = \int_0^t i(t-\tau)\sum_{j=-n}^{+N}\frac{1}{C_j}\exp\left\{\frac{-\tau}{R_jC_j}\right\}d\tau \qquad (14)$$

At this point, adjacent resistors and capacitors are taken to differ in value by respective factors, g^{-j} and G^{-j}. The values of the resistors and capacitors form respective geometric progressions.

$$R_j = g^{-j}R_0 \qquad (15)$$

and

$$C_j = G^{-j}C_0 \qquad (16)$$

Here g and G are the geometric factors, both of which are taken to be greater than unity. Eq (14) may be restated (21: 29) as

$$E_j(t) = \frac{R_0^{\nu}}{C_0^{1-\nu}} \int_0^t \frac{i(t-\tau)}{\tau^{\nu}} \sum_{j=-n}^{+N} \frac{\tau G^j g^j}{R_0 C_0} \exp\left\{\frac{-\tau G^j g^j}{R_0 C_0}\right\} d\tau \qquad (17)$$

where ν is defined as

$$\nu = \frac{\ln G}{\ln(Gg)} \qquad (18)$$

This definition limits ν to less than unity. In the limit as n and N both approach infinity and g and G both approach unity, Eq (17) may be written as (21: 29)

$$E(t) = \frac{\pi \csc(\nu\pi) R_0^{\nu}}{\Gamma(1-\nu) \ln(Gg) C_0^{1-\nu}} \int_0^t \frac{i(t-\tau)}{\tau^{\nu}} d\tau$$

$$= \frac{\pi \csc(\nu\pi) R_0}{\ln(Gg) C_0^{1-\nu}} \frac{d^{\nu-1}}{dt^{\nu-1}} i(t) = E_{id}(t) \qquad (19)$$

where the second equality is a consequence of the Riemann-Liouville definition of the fractional integral (21: 48). The ideal output voltage, E_{id}, is seen to be proportional to the $(\nu-1)$ differintegral of the input current. From the principle of continuity, the input current equals the output current, so if

a resistor is connected in series with this circuit, the voltage across the resistor, $E_R(t)$, is related to the input voltage E(t) by (10)

$$E_R(t) = i(t)\,R = \frac{\ln(Gg)\;C_0^{1-v}}{\pi\;\csc(v\pi)\;R_0^{v}}\;\frac{d^{v}E(t)}{dt^{v}} \qquad (20)$$

Because of the limit on v, the order of differentiation is limited to between 0 and 1. The exact order of the derivative is determined by the relationship between G and g, which do not necessarily approach unity at the same rate.

N and n were stipulated to be infinite in the derivation of Eq (19), but this requires using an infinite number of resistors and capacitors, which is not a realistic requirement when physically constructing a circuit. The requirement that g and G approach unity for each resistor-capacitor pair also results in an infinite number of components (21: 31). So that a circuit may be constructed, n and N are chosen to be much less than infinity, specifically n=N=2 for the case of v = 0.5, g = G = 2.57 (21: 32).These approximations result in upper and lower frequency bounds on the circuit, and cause some minor distortions within the bandpass of the circuit. However, within the bandpass the circuit still provides a reasonable approximation of a fractional order derivative.

The actual design of the circuit is somewhat complicated by the addition of an extra resistor-capacitor pair at each end of the circuit. These are added to help compensate for the infinite number of components that were truncated when finite n and N were selected, and much improve the performance of the circuit. For complete details, consult (21). Detailed information on the construction of the circuits is contained in Appendix A.

Oldfield-Burd-Doe Circuit

The second circuit examined was developed by Oldfield, Burd and Doe (19) for use in experimental heat transfer work. It is conceptually very similar to the Oldham-Zoski design, but has the advantage of considering real world component characteristics. Specifically, since it is much more difficult and expensive to obtain high-precision capacitors than resistors, this design makes allowances for capacitors that are only of minimal precision. The Oldfield-Burd-Doe (henceforth called OBD) design was done specifically to solve for the heat transfer rate in shock tube experiments. Specifically, the equations

$$\frac{\partial \dot{q}}{\partial x} = -\rho c \frac{\partial T}{\partial t} \tag{21}$$

and

$$\dot{q} = -k \frac{\partial T}{\partial x} \tag{22}$$

are solved for $\dot{q}$ in terms of T (in the Laplace domain) to yield

$$\dot{q}(s) = (\rho c k)^{\frac{1}{2}} T(s) s^{\frac{1}{2}} \tag{23}$$

where the $\dot{q}(s)$ and T(s) are Laplace transformed variables. From the discussion in section II, it is obvious that this equation has a solution containing a half order derivative. Since the designers of this circuit were

only interested in this one specific problem, the original development did not contain a parameter to allow for the design of an arbitrary order fractional derivative. Since this experiment chose a priori to use half order derivatives, this did not present a problem.

Whereas Oldham and Zoski allowed the progression of the resistors and capacitors in their design to vary independently, Oldfield, Burd and Doe designed a circuit where both progressions varied at the same rate, so g = G in this development. In exactly the same manner as Eq (18) this limits the order of the derivative to

$$v = \frac{\ln g}{\ln(g^2)} = \frac{\ln g}{2 \ln g} = \frac{1}{2} \tag{24}$$

The OBD circuit begins with the same assumption as before, that is, an infinite number of components continuously varying in resistance and capacitance. The basic circuit is arranged somewhat differently (Figure 3), but the result is the same.

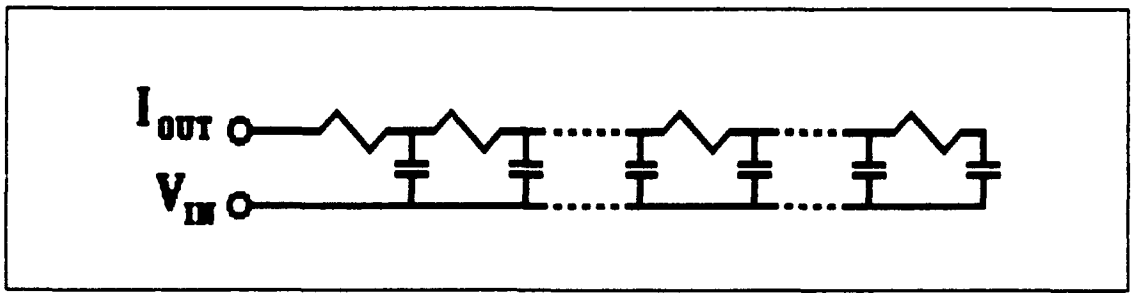

Figure 3. OBD "T-Section" Ladder

The complex impedance across such an infinite network is given by (19: 237)

$$Z(s) = \sqrt{\frac{r}{c}}\, s^{-\frac{1}{2}} \qquad (25)$$

Once again, the assumptions necessary for this result are relaxed to allow a finite number of components. Rather than a choosing an arbitrary geometric progression as Oldham and Zoski do, Oldfield chooses a progression for the capacitors so as to match commercially available components. One of the standard series of capacitors commercially available is (1.0, 2.2, 4.7, 10.0, 22.0, ...). By choosing the correct value for g ($10^{\frac{1}{3}}$), this progression can be approximated closely.

The Oldfield paper (19) showed experimentally that precise approximation of the infinite analog was not essential, as long as the correct relationship was maintained between adjacent resistor/capacitor pairs. Thus, rather than selecting a specific capacitance and trying to match it with various combinations of relatively inaccurate capacitors (21), they recommend selecting a single capacitor that is in the vicinity of the desired value, and then calculating the desired resistance to match it. Since resistors of five percent and even one percent accuracy are available commercially at relatively low cost, this is much easier and more inexpensive than trying to match both resistors and capacitors to predetermined values as the Oldham-Zoski circuit requires.

The OBD circuit requires some active components because the output of the network is the half order derivative of the output current rather than the output voltage as desired. From Ohm's law and Eq (23) it can follows that the output current of the circuit is related to the input voltage by

$$I(s) = \sqrt{\frac{C}{r}}\, E(s)\, s^{-\frac{1}{2}} \qquad (26)$$

A simple operational amplifier circuit known as a current-to-voltage converter (26: 439) transforms this into the desired voltage signal.

The current-to-voltage converter has an inverting configuration and causes the signal to be 180° out of phase. Also, the gain of the circuit is not as large as is desired. To match the theoretical fractional differentiator, the circuit should have a unity gain for an input signal with an angular frequency of one radian per second. Placing an inverting amplifier (26: 436) as the final component of the circuit corrects the phase shift and amplifies the output so that the circuit has the desired gain characteristics. The final configuration of the OBD circuit is shown in Figure 4. Details of the OBD construction can be found in Appendix B.

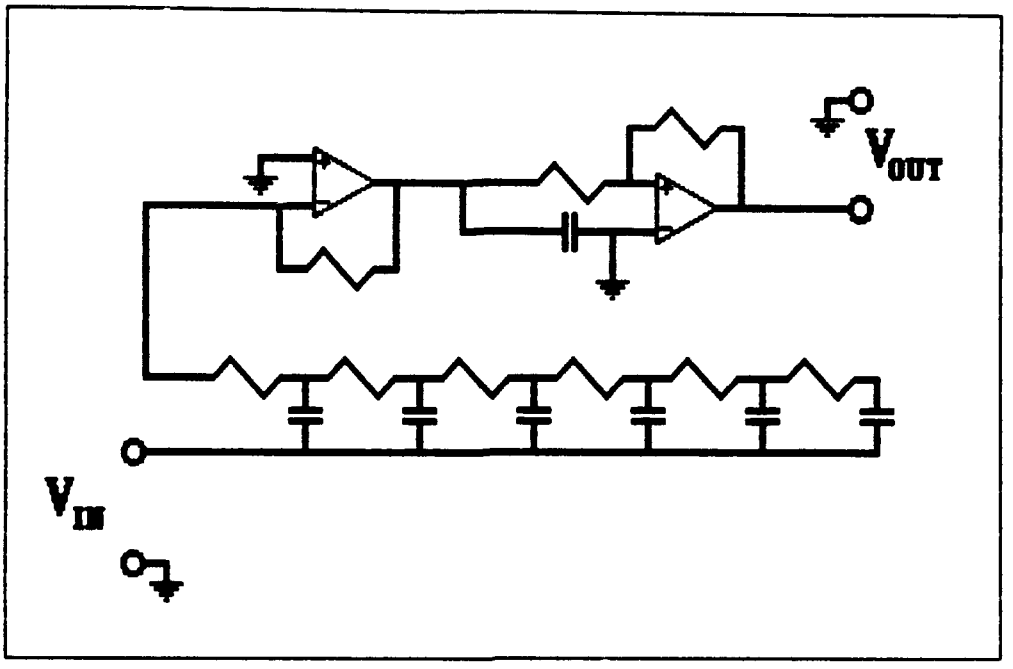

Figure 4. Schematic of OBD Fractional Differentiator

Characterization of Circuits

In order to decide which of these two circuit designs was superior, it was necessary to experimentally test the fabricated circuits and compare them to the ideal half-order differentiator. The ideal half-order differentiator has a 45° phase shift and 10 dB/decade slope on a Bode plot. To obtain a transfer function for each circuit, they were measured by a B&K 2032 Signal Analyzer with a band-limited pseudorandom noise input. Typical Bode plots for the half order Oldham-Zoski and OBD circuits are shown in Figures 5 and 6. Using similar components and care in construction, the OBD circuit was found to be more accurate than the Oldham-Zoski circuit,

and accurate over a wider frequency range. All further fractional differentiators were constructed according the OBD method.

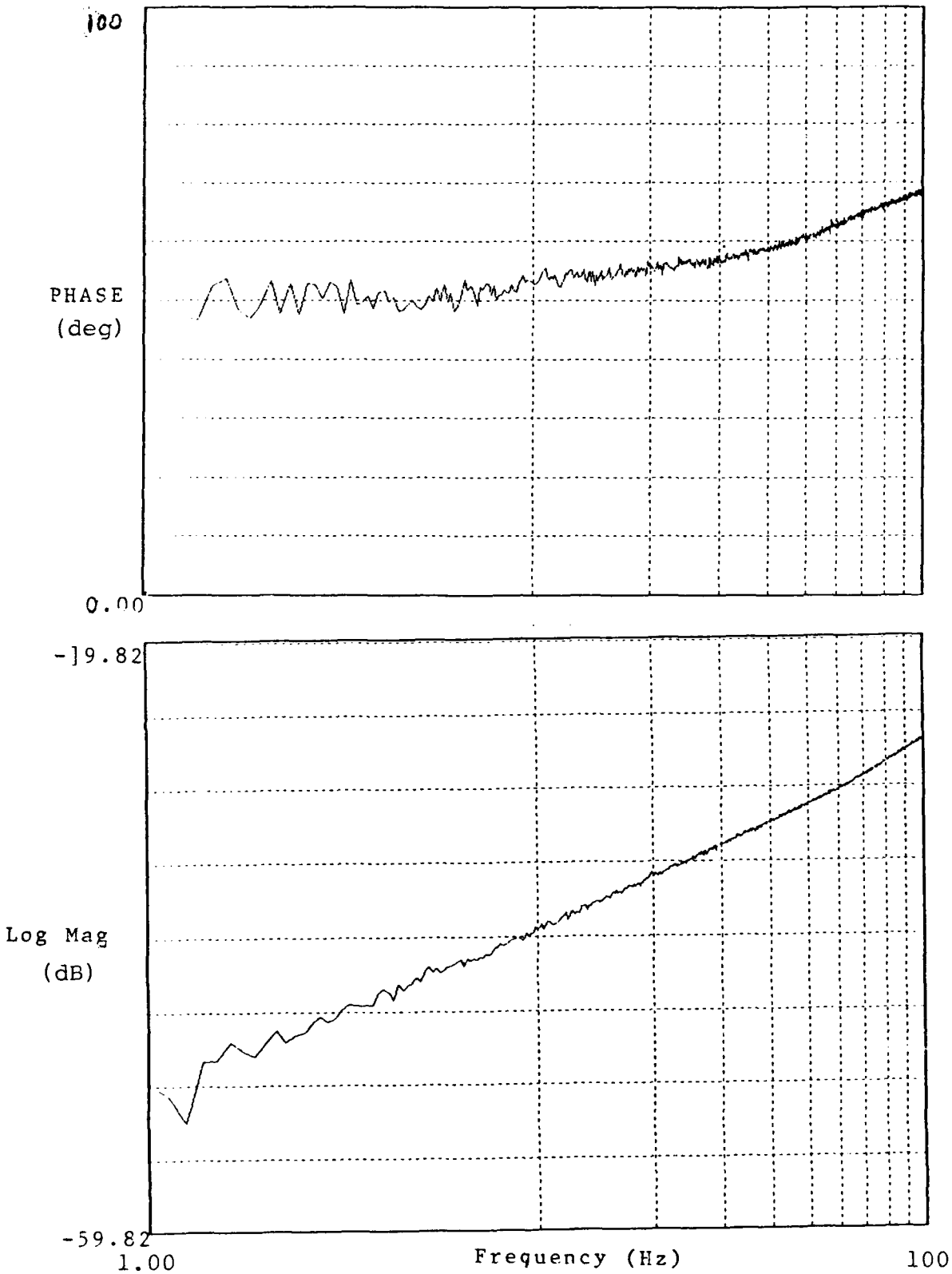

Figure 5. Frequency Response Function of Oldham-Zoski Circuit

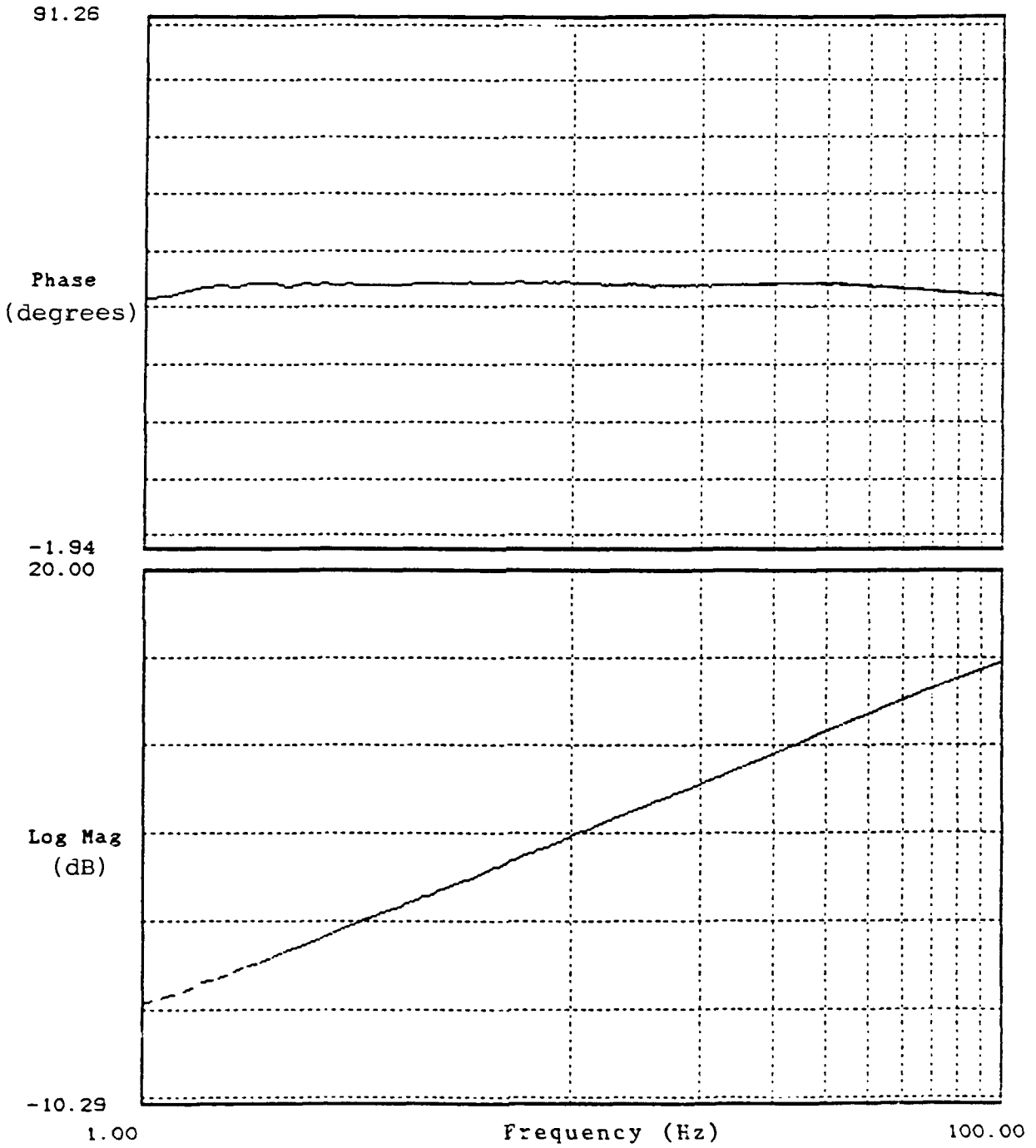

Figure 6. Frequency Response Function of OBD Circuit

IV. Characterization of Experimental Equipment

Overview

The structure studied in this experiment is a modification of the Advanced Beam Experiment originally developed by the Structural Dynamics branch of Wright Laboratory to study some of the problems associated with large space structures (13). It has low frequency, lightly damped modes of vibration that are closely spaced. In its original configuration, all components were selected with an eye towards eventually being implemented in a space environment, so proof-mass actuators were used to control the structure. Because of the numerous technical difficulties involved with these, they were replaced in this experiment by an electrodynamic shaker, which displayed much more regular behavior. Since the point of this particular research was to examine the effectiveness of fractional order feedback, and not to attempt to solve all the problems inherent in the control of large space structures, this was not a grave liability.

Structure

The structure used in this experiment is simply a six foot inverted cantilever beam with a 1" x 3/4" rectangular cross section. For this study the circular disc originally mounted at the base of the cantilever beam has been

removed. The structure is instrumented with two piezoresistive accelerometers and controlled by a single electrodynamic shaker. The beam is arranged as shown in Figure 7. The physical characteristics of the beam are shown in Table 1.

Table 1. Structure Physical Properties

Property Description	Value	Units
Beam Length (L)	70.75	in
Y Cross-Section Width (a)	1.01	in
Z Cross-Section Width (b)	0.758	in
Cross-Section Area (A)	0.7656	in^2
Young's Modulus (E)	10.8×10^6	lbf/in^2
Shear Modulus (G)	4.1×10^4	lbf/in^2
Beam Density (ρ)	2.591×10^{-4}	$lbf\text{-}sec^2/in^4$
Beam Mass (m_b)	1.403×10^{-2}	$lbf\text{-}sec^2/in$
Y Moment of Inertia (I_y)	3.667×10^{-2}	in^4
Z Moment of Inertia (I_z)	6.508×10^{-2}	in^4

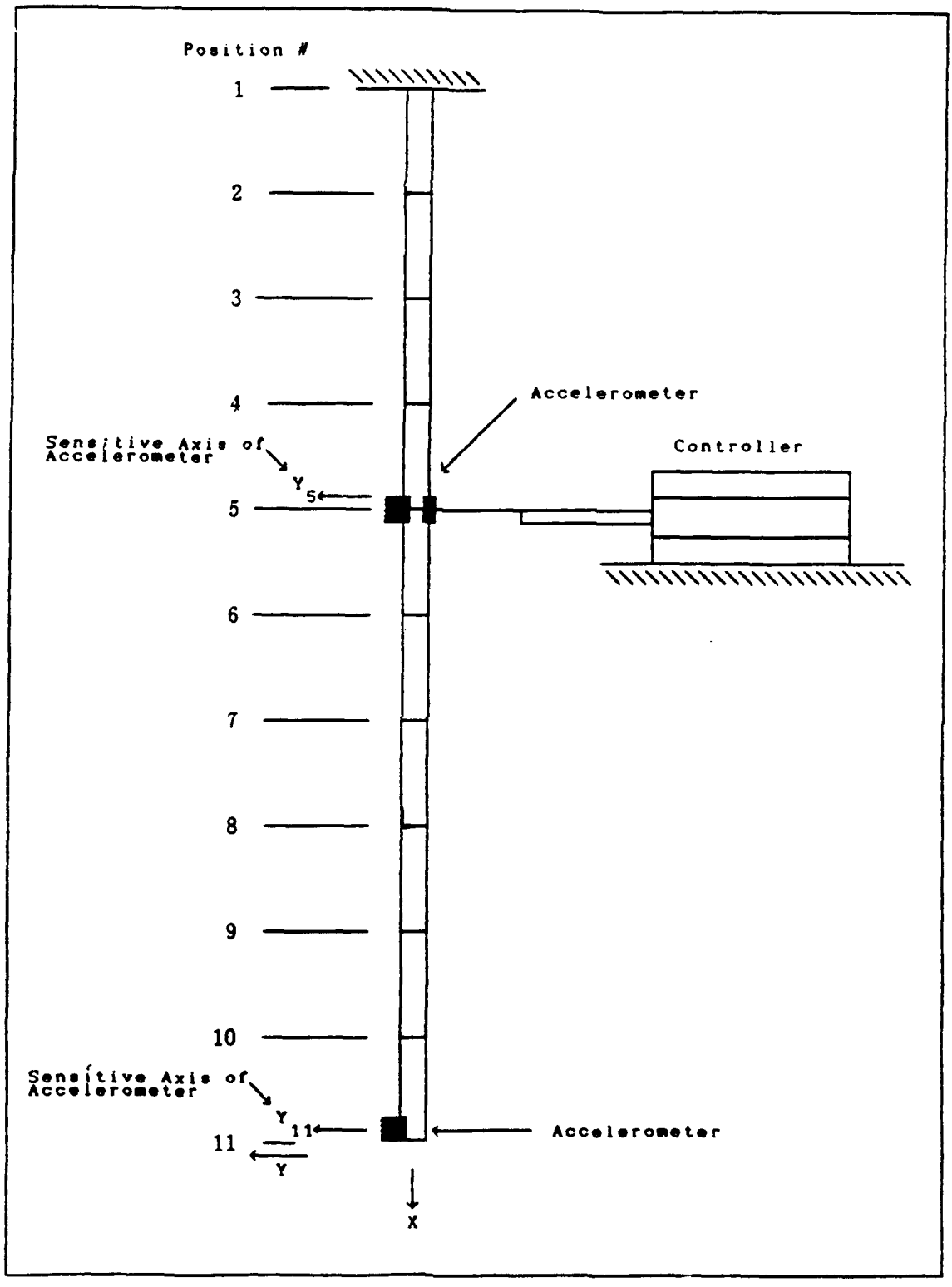

Figure 18. Diagram of Experimental Structure

Accelerometers

Because of the low frequencies of interest for this structure, piezoresistive accelerometers were chosen to measure the response of the beam. Piezoelectric accelerometers are more commonly used in vibration studies, but are not as effective at such low frequencies. The specific accelerometers used in this experiment were Endevco Model 2262 piezoresistive accelerometers with Endevco Model 4423 signal conditioners. These provide good low frequency response, and can actually make static (DC) measurements. The signal conditioners provide a zero adjustment so that the output of the accelerometers can be nulled before testing. For more details see (10) and (11).

Force Sensor

Force measurements were made with a B&K Model 8200 force gauge. Force measurements were used in the experimental modal analysis procedure, and taken off of an impact hammer used to excite the structure. When using an actuator to control a system it is common practice to measure the output of the actuator directly and feed that information back into the controller. This is done because many actuators display some sort of nonlinear behavior at some point in their response, and there may be a substantial difference between the commanded input and the input the actuator actually applies to the system. In order to best control the system, it

is necessary to know precisely what forces are acting on the system to effect its reponse. Because we have only one force sensor available for this experiment, the actuator was calibrated with the force sensor, but run open-loop in the tests. The actuator used is very nearly linear in the frequency bandwidth of interest so this did not prove to be a problem for this experiment.

Actuation

The only actuator used in this experiment is an APS Model 113-LA Structural Dynamics Shaker, driven by an APS Model 114 dual mode power amplifier. This shaker is ideal for work in low frequency vibration studies because of its long stroke limit of six inches and its light weight armature, which minimizes its influence on lightweight structures. The shaker's force output is linear in the frequency range of this system (Figure 8), so it was possible to run it open-loop, with no force measurement fed back from the attachment point. For more details, see (1) and (2).

Digital Controller

The controller for this experiment is the PC-1000 Systolic Array Processor, which is a sixteen channel digital controller. It has internal analog-to-digital (A-D) and digital-to-analog (D-A) converters, and allows input and output gains to be set for each channel. It has a maximum sampling rate of 2000 Hz, which was the rate chosen for this experiment.

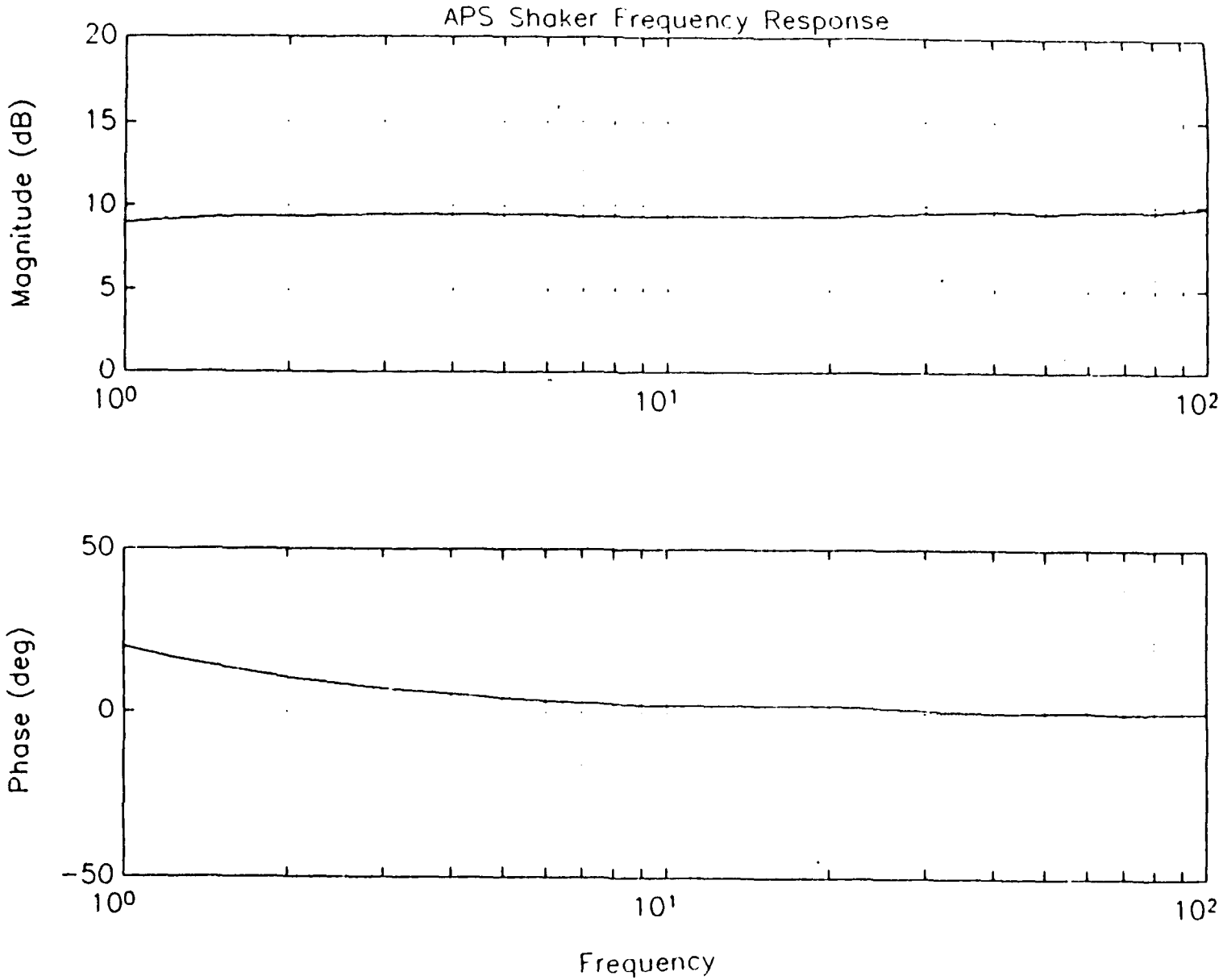

Figure 8. Actuator Frequency Response Curve

The controller is programmed via a GPIB connection to a PC. For more details see (27).

Modeling

One of the fundamental difficulties in designing any control system is developing a mathematical model that adequately represents the physical system to be controlled, and this problem proved to be no exception. For the purposes of this experiment only bending motion in one axis was studied, and it was assumed to be uncoupled to bending motion in the other axis or to torsional motion. The original intention was to use a 22 degree-of-freedom finite element model that had been previously developed for the structure by Yang (30). This model looked at displacements and rotations at eleven points on the beam, with point masses representing the accelerometers and the shaker armature. The model was iteratively tuned by varying a linear and torsional spring constant at its base until it produced good agreement for the experimentally measured natural frequencies of the first two modes. Details of the model are shown in Appendix F. However, controllers that were designed using this model had very poor performance when actually tested on the structure.

A closer comparison between the model and experimental data showed that the model was only accurate for the first two modes, and of varying accuracy for the other twenty modes. In this case the LQ regulator (designed in spatial variables) weighted all modes equally when looking for a solution. The resulting controllers had a very wide bandwidth, which tends to make a system very susceptible to any noise present in the feedback.

Since only the first two bending modes were to be controlled, it was decided to reduce the model to reflect this. This model would only look at the two positions where accelerometers were present. The original stiffness matrix, $\mathbf{k_o}$, taken from the finite-element model, was reduced by first inverting it to find the compliance matrix, then picking out the four terms that affected the x_5 and x_{11} positions. This 2 by 2 matrix was then inverted to find the reduced stiffness matrix, $\mathbf{k}$.

$$\mathbf{k} = \begin{bmatrix} 263.87 & -54.82 \\ -54.82 & 17.35 \end{bmatrix} \text{(lb/inch)} \tag{27}$$

To produce a better representation of the actual behavior of the structure, it was decided to calculate a reduced mass matrix, $\mathbf{m}$, and a reduced damping matrix, $\mathbf{c}$, using the first two mode shapes, the natural frequencies, and the resonant response determined experimentally. The mode shapes are calculated from the imaginary portion of the transfer function (12: 195-198). Details are shown in Appendix F.

To begin with, it is necessary to show the relationship between the displacement formulation and the modal formulation of the problem. The displacement formulation is based on a physically measurable displacement vector, $\underline{z}$. For a damped N degree-of-freedom system, the motion is described by

$$\mathbf{m}\ddot{\underline{z}} + \mathbf{c}\dot{\underline{z}} + \mathbf{k}\underline{z} = \mathbf{D}\underline{u} \tag{28}$$

For this problem, u, the force input to the structure, is a scalar quantity. D shows at which coordinate the control force is being applied.

$$D^T = [\,1 \quad 0\,] \tag{29}$$

There is an equivalent formulation written in modal coordinates, which are related to the physical displacements by

$$z = \Phi \eta \tag{30}$$

where η is the vector of modal displacements and Φ is the modal matrix composed of the eigenvectors of the open loop system. The equivalent description is written as

$$I\ddot{\eta} + [2\zeta_n w_n]\dot{\eta} + [w_n^2]\eta = \Phi^T D u \tag{31}$$

where $[2\zeta_n w_n]$ and $[w_n^2]$ are diagonal matrices containing the associated values for each mode. This formulation presupposes that the modal matrix, Φ, has been scaled so that

$$\Phi^T m \Phi = I \tag{32}$$

Comparing Eq (28) and Eq (31) shows that k must be equal to

$$\Phi^T k \Phi = [w_n^2] \tag{33}$$

So having determined Φ and $[w_n^2]$ experimentally, and with the $\mathbf{k}$ calculated in Eq (27) it becomes possible to scale the Φ so that Eq (33) is approximately true. There are only two parameters to vary, the scaling factors for each mode shape, so it is in general not possible to force the diagonal terms to zero in Eq (33). It is possible to scale Φ such that the diagonal terms are met exactly. By rearranging Eq (32) it is now possible to calculate an $\mathbf{m}$ that satisfies the experimentally measured data.

$$\mathbf{m} = (\Phi^T)^{-1}\,\Phi^{-1} = \begin{bmatrix} 9.28 & 1.83 \\ 1.83 & 2.74 \end{bmatrix} \times 10^{-3} \left(\frac{\text{lbf}\ s^2}{\text{in}} \right) \tag{34}$$

Similarly, it is possible to calculate a damping matrix, $\mathbf{c}$, using the scaled Φ and the diagonal matrix $[2\zeta_n w_n]$

$$\mathbf{c} = (\Phi^T)^{-1}\,[2\zeta_n w_n]\,\Phi^{-1} = \begin{bmatrix} 3.46 & 1.69 \\ 1.69 & 1.66 \end{bmatrix} \times 10^{-3} \left(\frac{\text{lbf}\ s}{\text{in}} \right) \tag{35}$$

In order to use the tools available from modern control theory, it is necessary to put Eq (28) into the standard state space form of

$$\dot{\underline{x}} = A\underline{x} + B\underline{u} \tag{36}$$

where $\underline{x}$ is defined as the state vector composed of $\dot{\underline{z}}$ and $\underline{z}$, and $\mathbf{A}$ and $\mathbf{B}$ have the form

$$\mathbf{A} = \begin{bmatrix} \mathbf{0} & \mathbf{I} \\ -\mathbf{m}^{-1}\mathbf{k} & -\mathbf{m}^{-1}\mathbf{c} \end{bmatrix} = \begin{bmatrix} 0 & 0 & 1 & 0 \\ 0 & 0 & 0 & 1 \\ -37300 & 8240 & -8.22 & 0.606 \\ 44800 & -11800 & 3.56 & -5.95 \end{bmatrix} \quad (37)$$

$$\mathbf{B}^T = [0 \;\; 0 \;\; \mathbf{m}^{-1}\mathbf{D}] = [\; 0 \quad 0 \quad 124 \quad -82.7 \;] \quad (38)$$

The product $-\mathbf{m}^{-1}\mathbf{k}$ was calculated from the definitions of m and k in Eqs (32) and (33).

$$-\mathbf{m}^{-1}\mathbf{k} = -((\Phi^T)^{-1}\Phi^{-1})^{-1}(\Phi^T)^{-1}[w_n^2]\Phi^{-1}[w_n^2] = -\Phi[w_n^2]\Phi^{-1} \quad (39)$$

To verify the accuracy of the model, the open-loop transfer function computed from this model is plotted against the experimentally determined open-loop transfer function in Figure 9. All transfer functions derived from the experimental structure shown in this work will be accelerances $\left(\frac{Z(s)}{F(s)}\right)$, with the force measurement taking place at the midpoint of the beam where the actuator is located (x_5), and the acceleration measurement taking place at the tip accelerometer (x_{11}). The models show reasonable agreement in terms of the both the frequencies and dampings for both modes, but the magnitudes are off by a significant amount.

The most likely source of the magnitude error is the poor accuracy of the measurement technique at low frequency. The structure has bending modes in the other lateral direction and torsional modes as well, all within the bandwidth of interest. The frame supporting the structure has modes occuring in that frequency range as well. The theoretical model

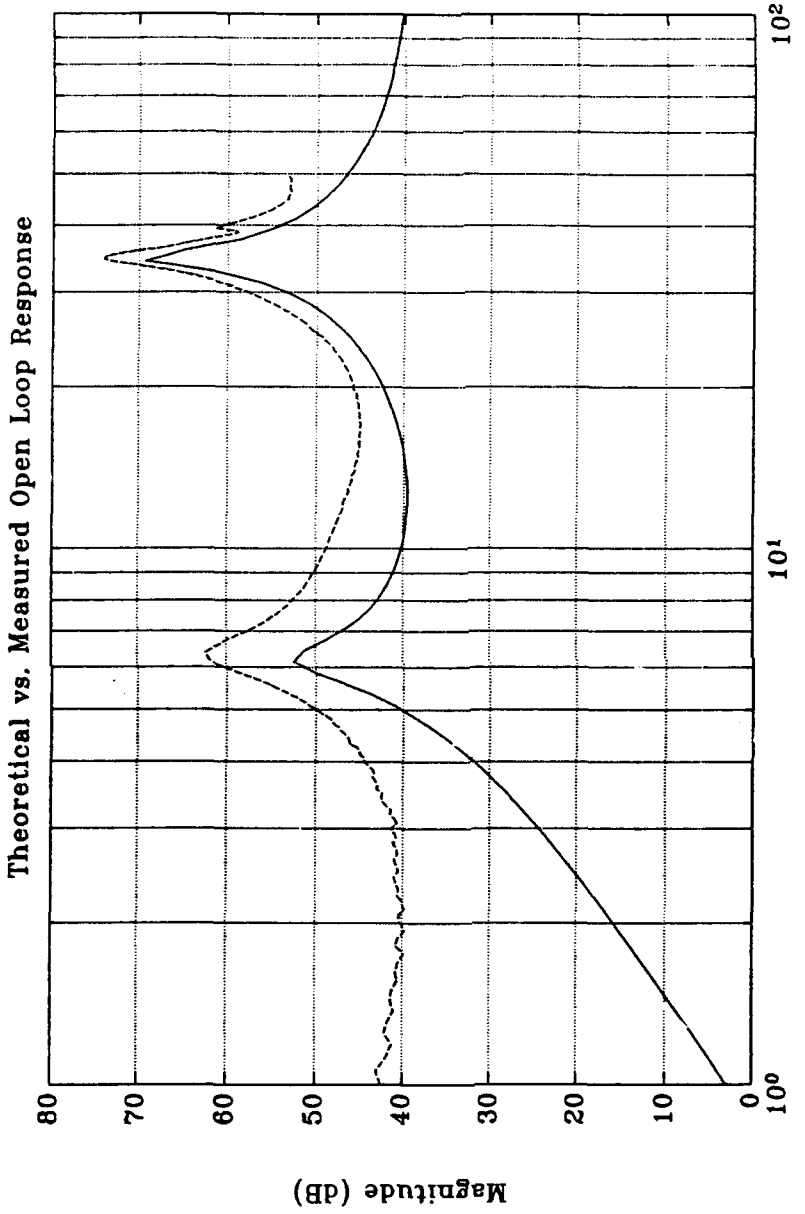

Figure 9. Comparison of Open-Loop Transfer Functions

displays the expected behavior of a two degree of freedom system, with the slope approaching 40dB/decade at low frequencies and the measurement has been checked thoroughly. The logical conclusion is that the structure's response is not well represented by a second order mass and stiffness model. To better represent the behavior of the structure within the desired frequency range, higher order models should be examined.

V. Measurement Channels

Overview

A major source of difficulty in performing this experiment was the construction and troubleshooting of the measurement channels. The signal from the beam is acquired as an acceleration, then it is variously integrated, differentiated, and filtered to obtain the requisite position, velocity, and fractional derivative feedback signals. A diagram of the entire process is shown in Figure 10.

Integration Circuits

The integration circuits used in this experiment were originally built by Jacques (13) for his thesis work, based on a design provided by the Structural Dynamics Branch, Wright Laboratory (shown in Figure 11). This design provides good performance for integration above 1 Hz, and attenuates inputs below 0.1 Hz, where the pole of the integrator is located.

High-Pass Filters

To obtain the position measurements required for full-state feedback, the output of the accelerometers had to be passed through two successive integration processes. Theoretically there is no reason why this should present a problem, nevertheless, when non-ideal components were used

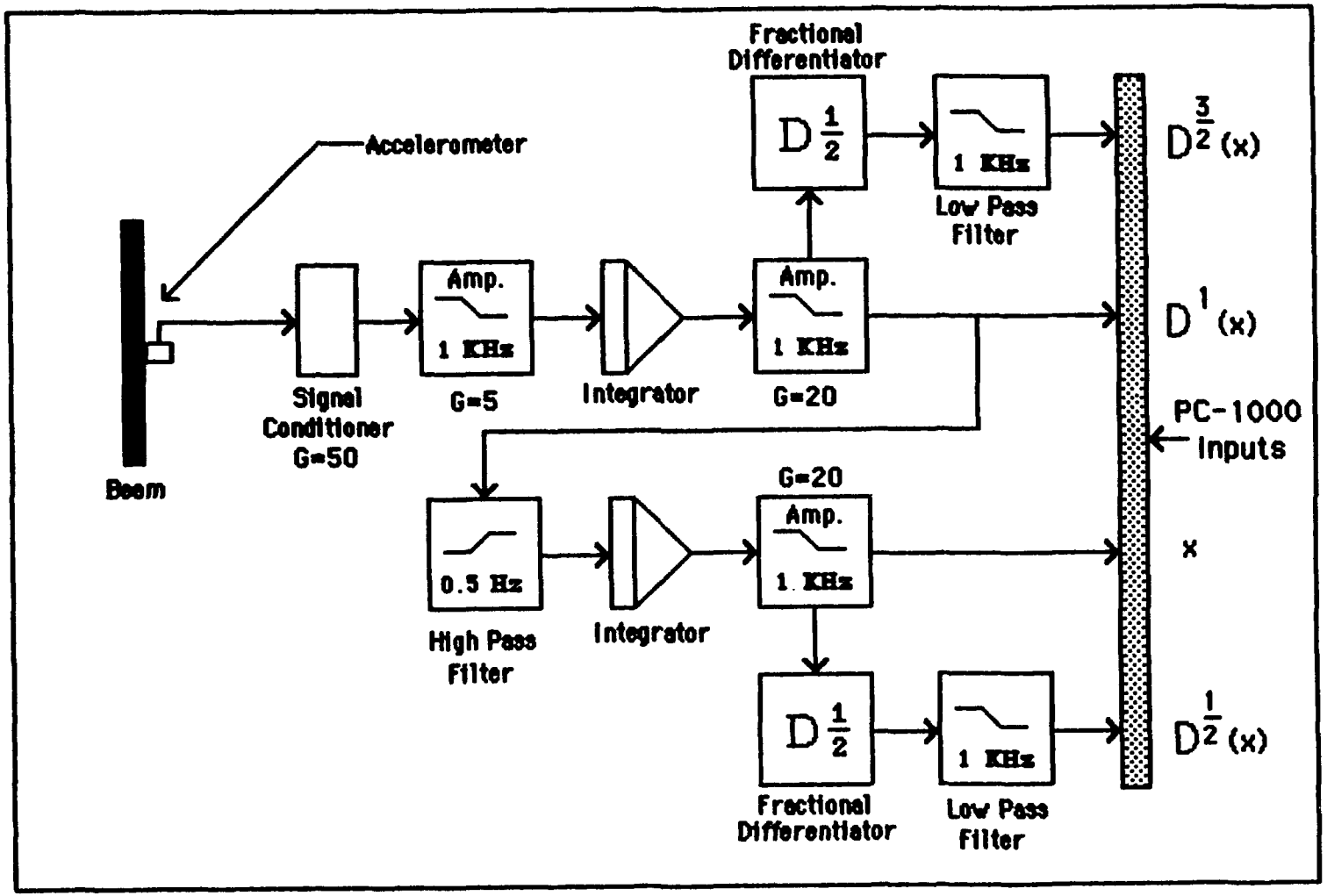

Figure 10. Measurement Channel Diagram

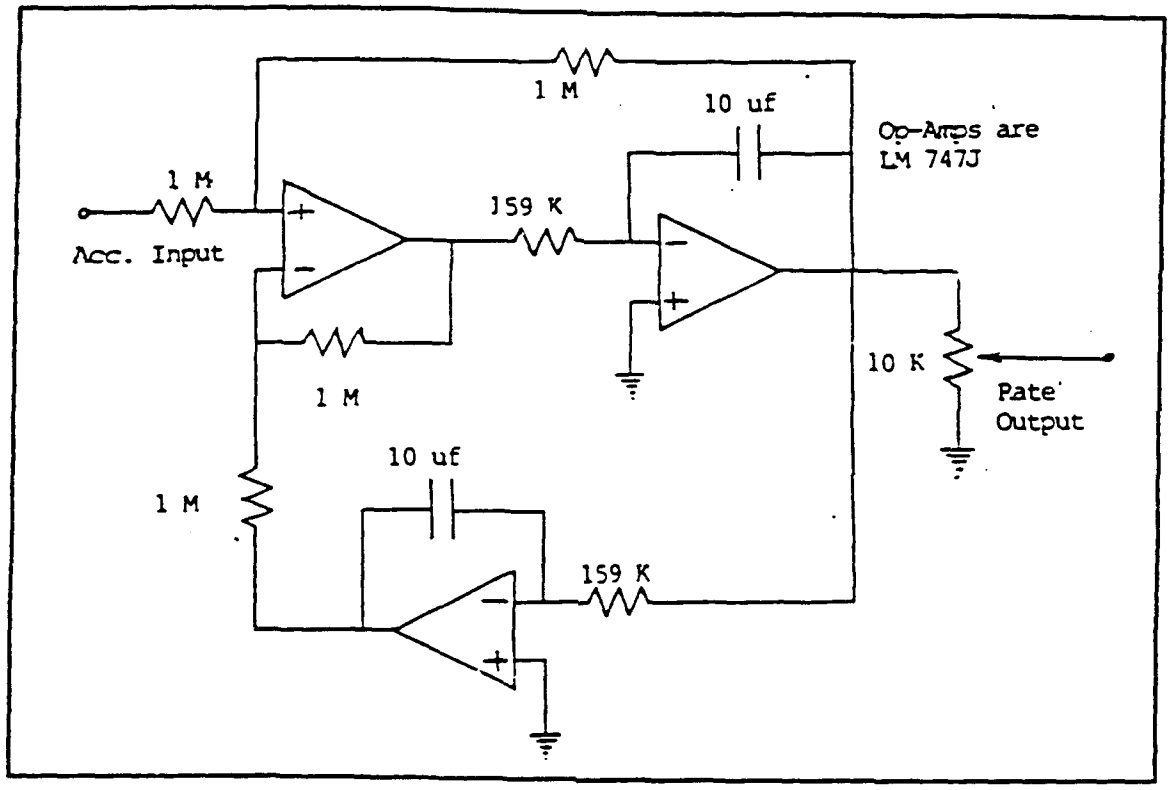

Figure 11. Integration Circuit Diagram

there was a complication. Real integrators are normally constructed with a transfer function of the form $\frac{1}{s + b}$, as opposed to that of the ideal integrator, which is $\frac{1}{s}$. When two integrators were cascaded (the output of one fed into the other), the transfer function for the system is of the form

$$G(s) = \frac{1}{s^2 + 2bs + b^2} \qquad (35)$$

From the theory developed to study second-order systems, this corresponds to

$$G(s) = \frac{1}{s^2 + 2\zeta w_n s + w_n^2} \tag{41}$$

Comparing these two expressions reveals that b is equal to the natural frequency (w_n) of the system and that the system is critically damped ($\zeta = 1$). The settling time for such a system, T_s, is defined as the time required for the system to settle within a certain percentage of the amplitude of an input step function. For a 2% settling time this is approximately (18: 236-237)

$$T_s \approx \frac{4}{\zeta w_n} = \frac{4}{(1)(.1)} = 40 \text{ seconds} \tag{42}$$

Since the fastest mode of vibration of interest in this structure is 35 Hz, this is much too long a settling time for the position measurement taken to be of any possible use. In fact, the inherent damping present in the beam would cause it to settle before an initial measurement of its motion would!

The solution to this problem lay in a closer examination of the phenomena involved. The resonance in the first integrator is feeding directly into the second integrator and causing a "ringing" in the circuit. To avoid this, a high-pass filter is placed between the first integrator and the second to filter out the response in the vicinity of 0.1 Hz.

Because of the rapid roll-off (the rate of attenuation of a signal with a frequency outside of the pass band) required of the filter, it was not practical to build a passive filter for this experiment. There are many possible choices of active filter designs available, including elliptic, parabolic,

Bessel, Papoulis, Gaussian, and Butterworth filters (24), all of which were considered at one time or another.

Unfortunately, the filter creates another problem. Active electronic components do not function well as their inputs approach direct current (0 Hz). Also, in order to minimize the phase distortion of the input signals the corner frequency of the filter must be placed approximately two decades below the lowest frequency of interest. As initially configured, the structure had a first mode bending frequency of 2.1 Hz, and it proved impossible to build a filter that did not distort the phase of the first mode signals by an unacceptable amount. To work around this, the structure was physically modified by removing a plate that had been attached to the bottom of the beam. This raised the first mode frequency to 6.3 Hz, and filters were able to be constructed that better preserved the phase information at that frequency.

To improve the roll-off of a filter, one would normally build a higher order filter (add more poles to the filter). However, because of the extremely low frequencies involved, this strategy did not work. In fact, when the filter order was changed from second to third order (or higher) the performance actually deteriorated. Since optimal performance seemed to occur with the second order filters, it was necessary to choose a filter design that had the highest inherent roll-off. Chebyshev filters (24) have a higher roll-off than the other filter designs considered, but cause a small ripple in the magnitude of the pass band. This was deemed to be an acceptable design trade-off.

A Chebyshev filter has a transfer function based on a Chebyshev polynomial appearing in the denominator of the transfer function. A Bode

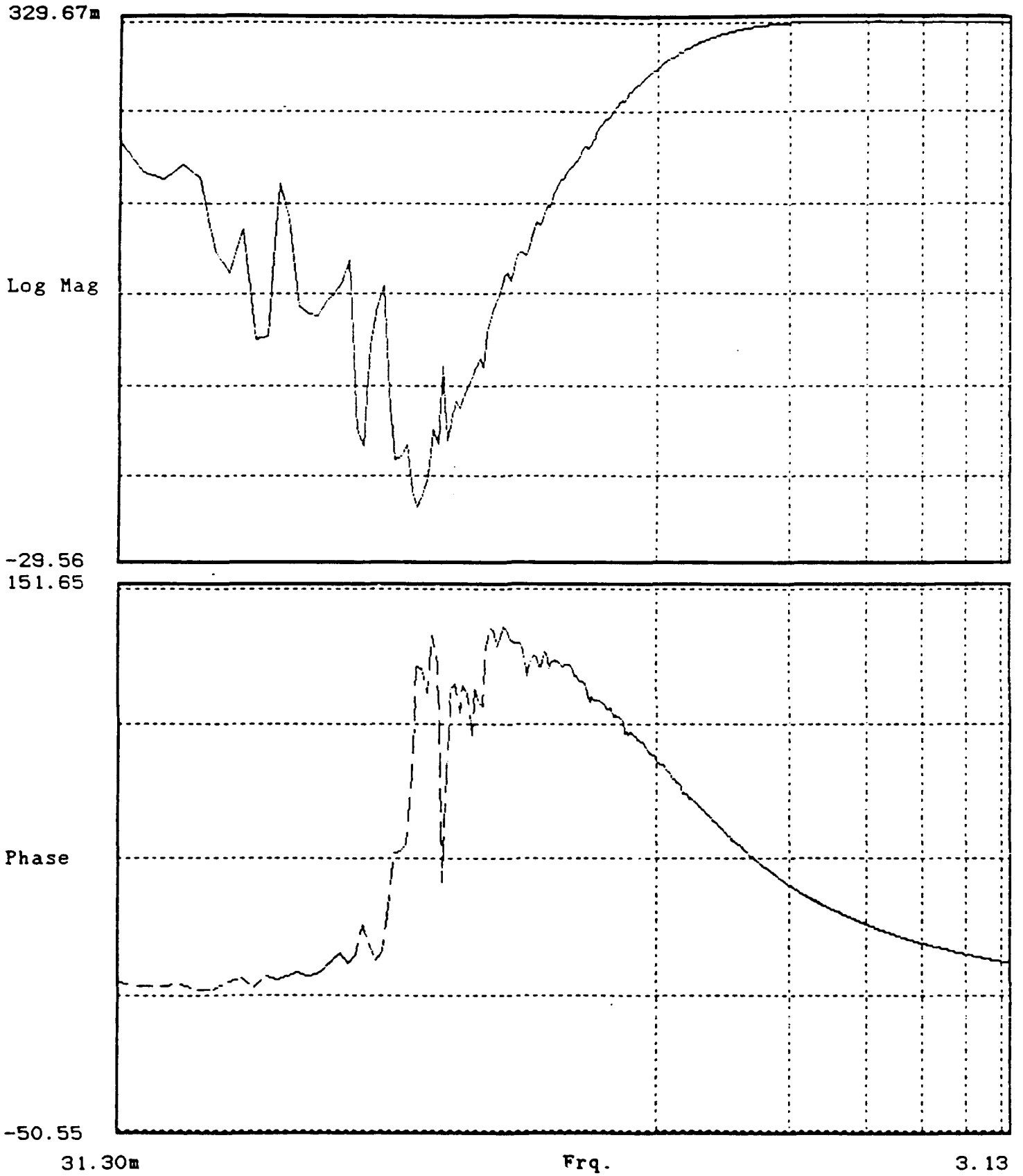

Figure 12. Frequency Response of High-Pass Filter

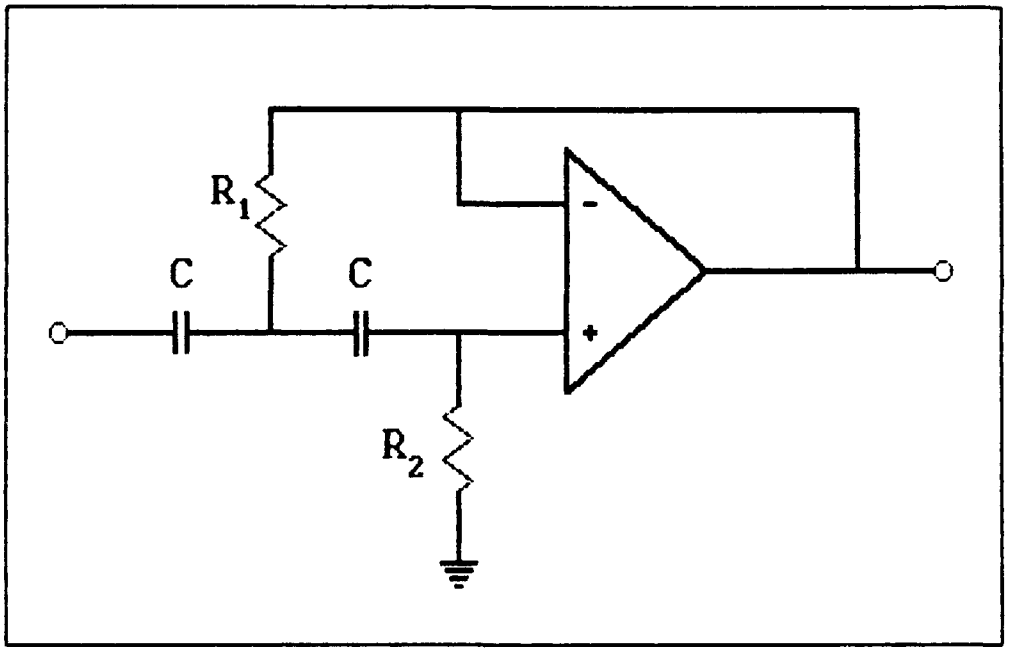

Figure 13. High Pass Filter Circuit Diagram

plot of one of the filters used is shown in Figure 12. A circuit diagram of a second order Chebyshev filter is shown in Figure 13. Specific details of the construction are included in Appendix C.

Low-Pass Filters

When the fractional state inputs were first fed back from the structure and the controller was turned on, the system was found to be only marginally stable, with audible high frequency resonances occuring. When these where characterized, it was found that the structure was resonating at harmonics of the sampling frequency of the digital controller. The problem was finally traced to the high frequency behavior of the fractional

differentiator circuits, which did not roll-off until approximately 15 KHz. (See Figure 14.) The differentiators amplify any high frequency noise by the square root of its frequency. Any small amount of high frequency noise entering the fractional differentiators had its magnitude amplified greatly, and this dominated the sample taken at every period.

The solution to this probem was to low-pass filter the fractional state channels just prior to entering the PC-1000 so that there was at least 20 dB of roll-off at 1000 Hz. Once again, there is a design trade-off between preserving the phase information at the frequencies of interest and still getting the necessary roll-off. For this problem, second order Butterworth (20) low-pass filters were chosen and built. These filters are similar to the Chebyshev high-pass filters discussed earlier, with only a few minor differences.

The Butterworth filters are constructed so the transfer function matches a Butterworth polynomial. The circuit diagram is identical to Figure 13, except that the resistors and capacitors are interchanged. Finally, the Butterworth filter has a flat pass-band, so there is none of the ripple present associated with Chebyshev filters. A Bode plot of one of the filters used is shown in Figure 15. Details of construction are presented in Appendix D.

Final Measurement Channels

To maximize the accuracy of the feedback signals, it was desirable to amplify the signals at several points to counteract attenuation caused by the integration process. The PC-1000 has an internal analog-to-digital converter, and it was necessary to ensure that the input signals at that point be near

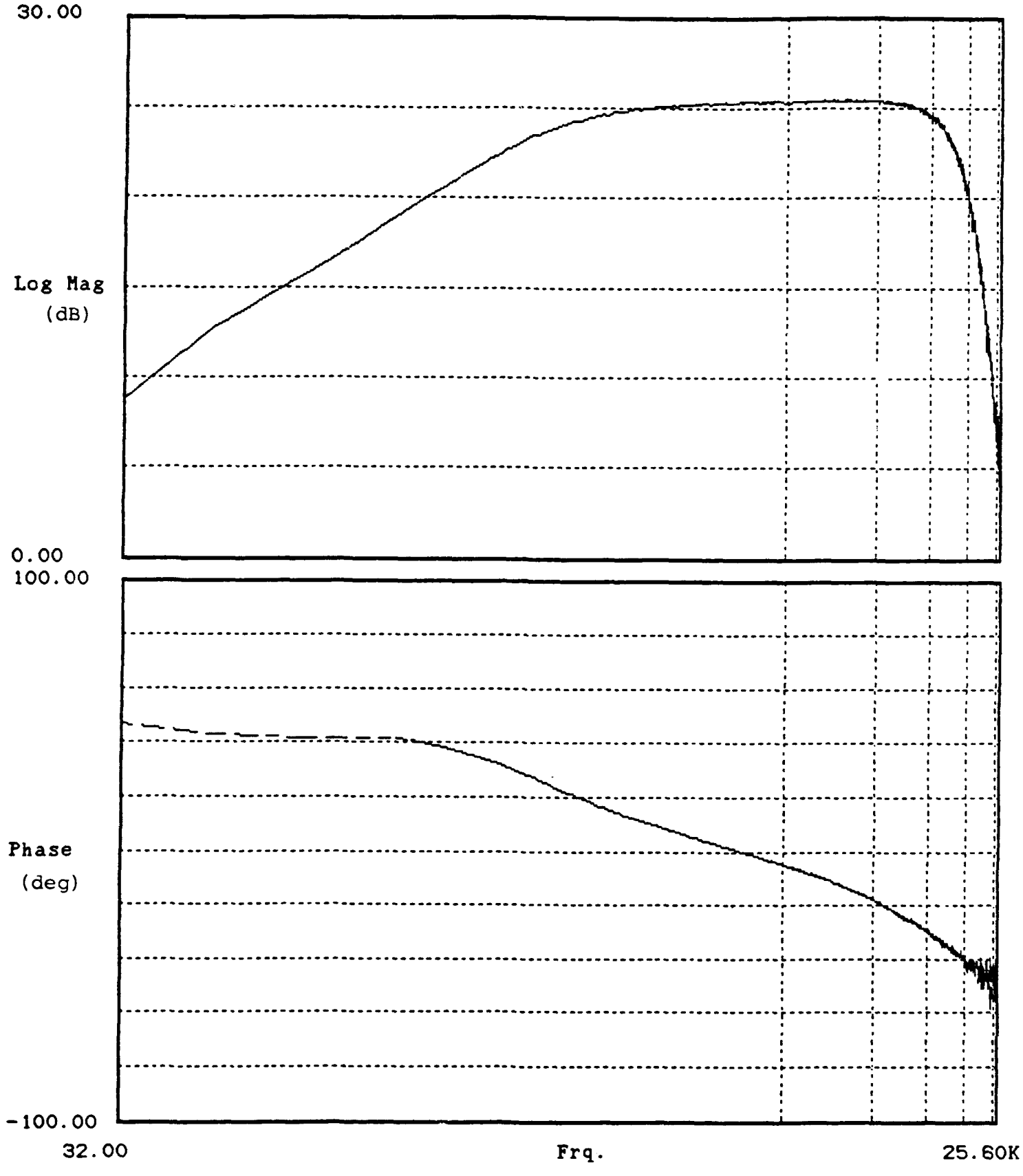

Figure 14. High Frequency Response of 1/2 Differentiator

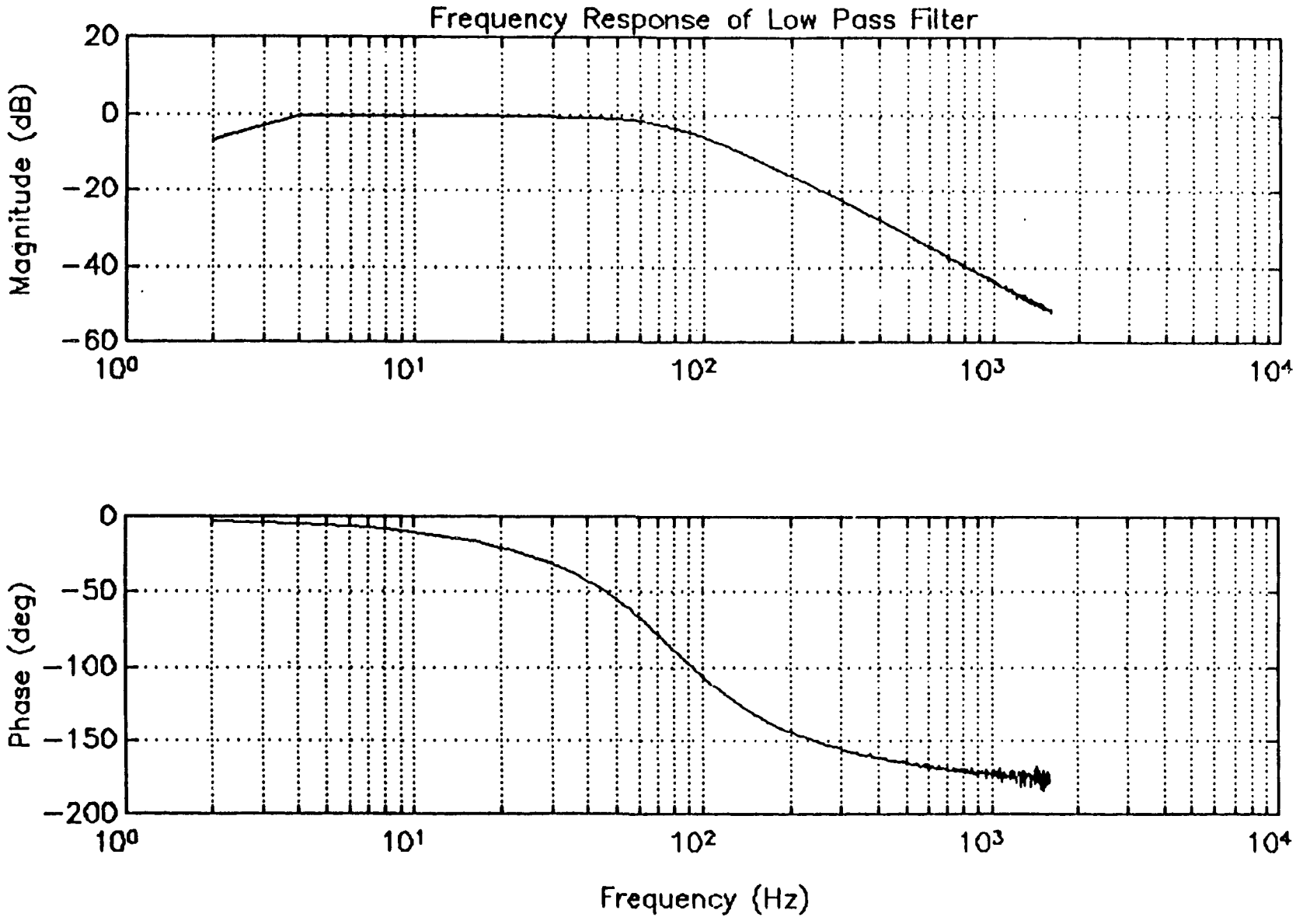

Figure 15. Frequency Response of Butterworth Low-Pass Filter

the minimum full scale range. To avoid saturating the integrators and clipping the signals, it was necessary to provide amplification in several stages. To avoid the sampling probems discussed above for the velocity and position feedback, the low-pass filters built into the amplifiers for those channels were set to 1 KHz.

Since there were a variety of components cascaded together in each channel, it was decided to calibrate the entire feedback channel at once. Block diagrams for the four different signals are shown in Figure 10. The circuits were calibrated from the point where the signal from the accelerometers leaves the signal conditioners to the where the signal was finally input to the PC-1000.

The calibration was performed by using the B&K 2032 and its random signal generator to generate the plots of the frequency response for each channel. The theoretical magnitude of each channel can be calculated at a frequency by $G_{th} = \frac{1}{w^v}$, where v is the order of integration of the channel. This theoretical value was calculated for an average frequency of the system bandwidth. This number was divided by the measured value at the same frequency, and multiplied by the accelerometer calibration constants to obtain the final gain for each channel. The calibrated gains for each channel are listed in Table 2.

The final frequency response plots of each of the types of measurement channel are shown in Figures 16-19. The high pass filter before the second integrator is responsible for the low frequency phase distortion present in the x and $D^{\frac{1}{2}}(x)$ channels. The phase distortion at higher frequencies in the fractional order channels caused by the low pass filters is also particularly

noticeable. However, the magnitude plots all exhibit near ideal behavior in the frequency interval of interest.

Table 2. Measurement Channel Gains.

Channel Number	Signal	Gain	Units
1	$D^1(x_1)$	7.67	in sec^{-1} V^{-1}
2	$D^1(x_2)$	7.19	in sec^{-1} V^{-1}
3	x_1	.288	in V^{-1}
4	x_2	.277	in V^{-1}
5	$D^{\frac{1}{2}}(x_1)$	1.289	in $sec^{-\frac{1}{2}}$ V^{-1}
6	$D^{\frac{1}{2}}(x_2)$	2.915	in $sec^{-\frac{1}{2}}$ V^{-1}
7	$D^{\frac{3}{2}}(x_1)$	11.6	in $sec^{-\frac{3}{2}}$ V^{-1}
8	$D^{\frac{3}{2}}(x_2)$	31.95	in $sec^{-\frac{3}{2}}$ V^{-1}

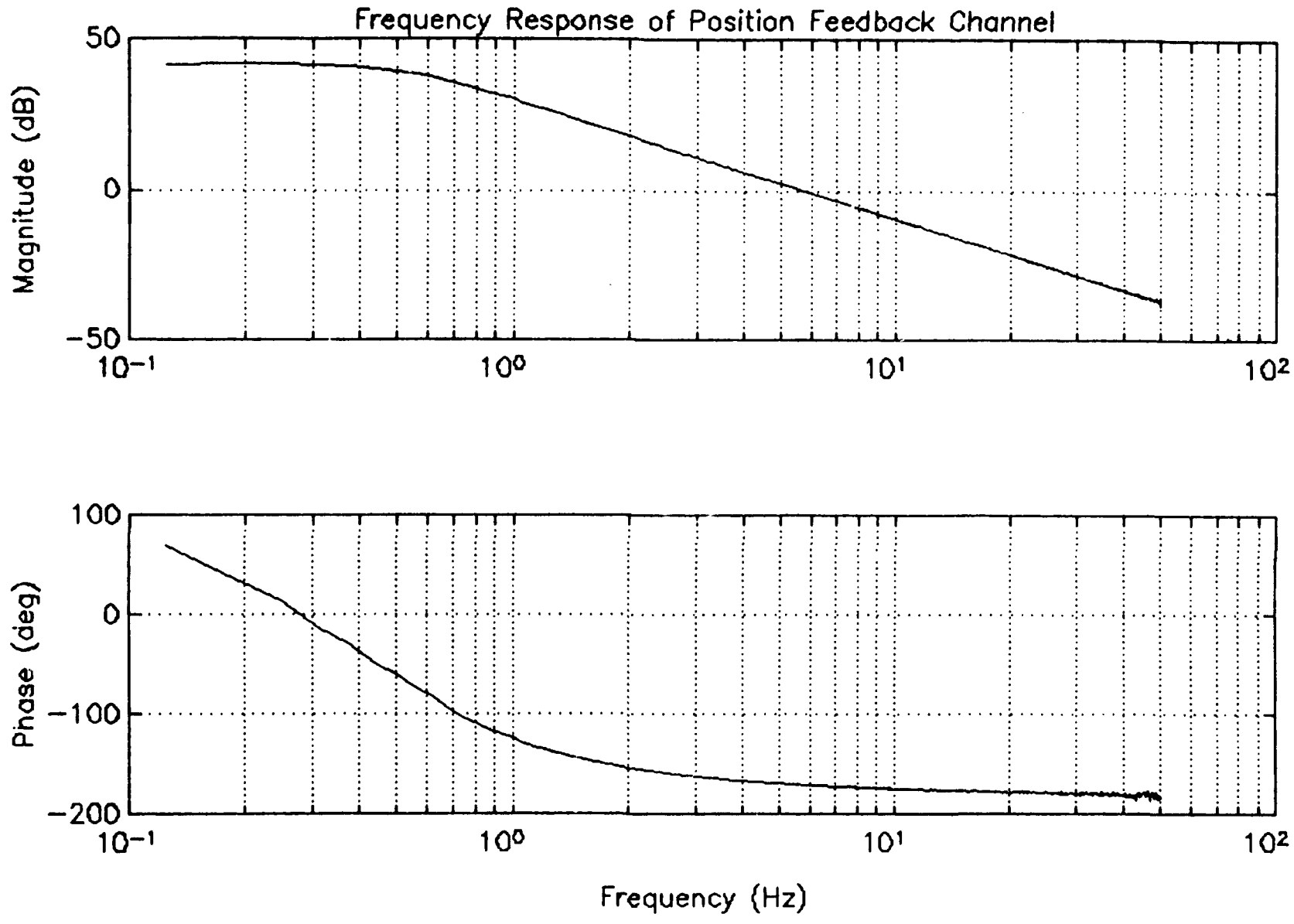

Figure 16. Frequency Response of Position Feedback Channel

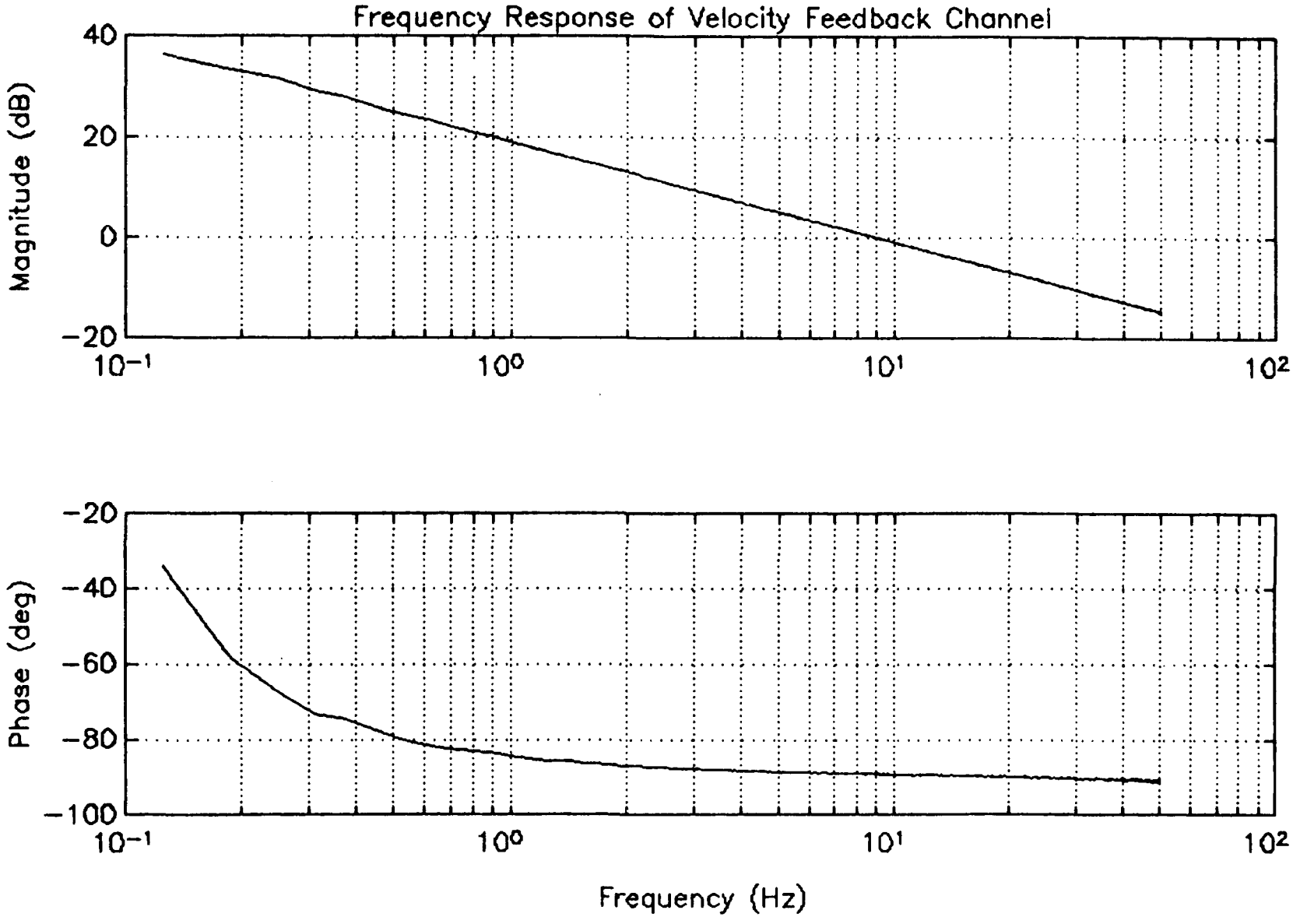

Figure 17. Frequency Response of Velocity Feedback Channel

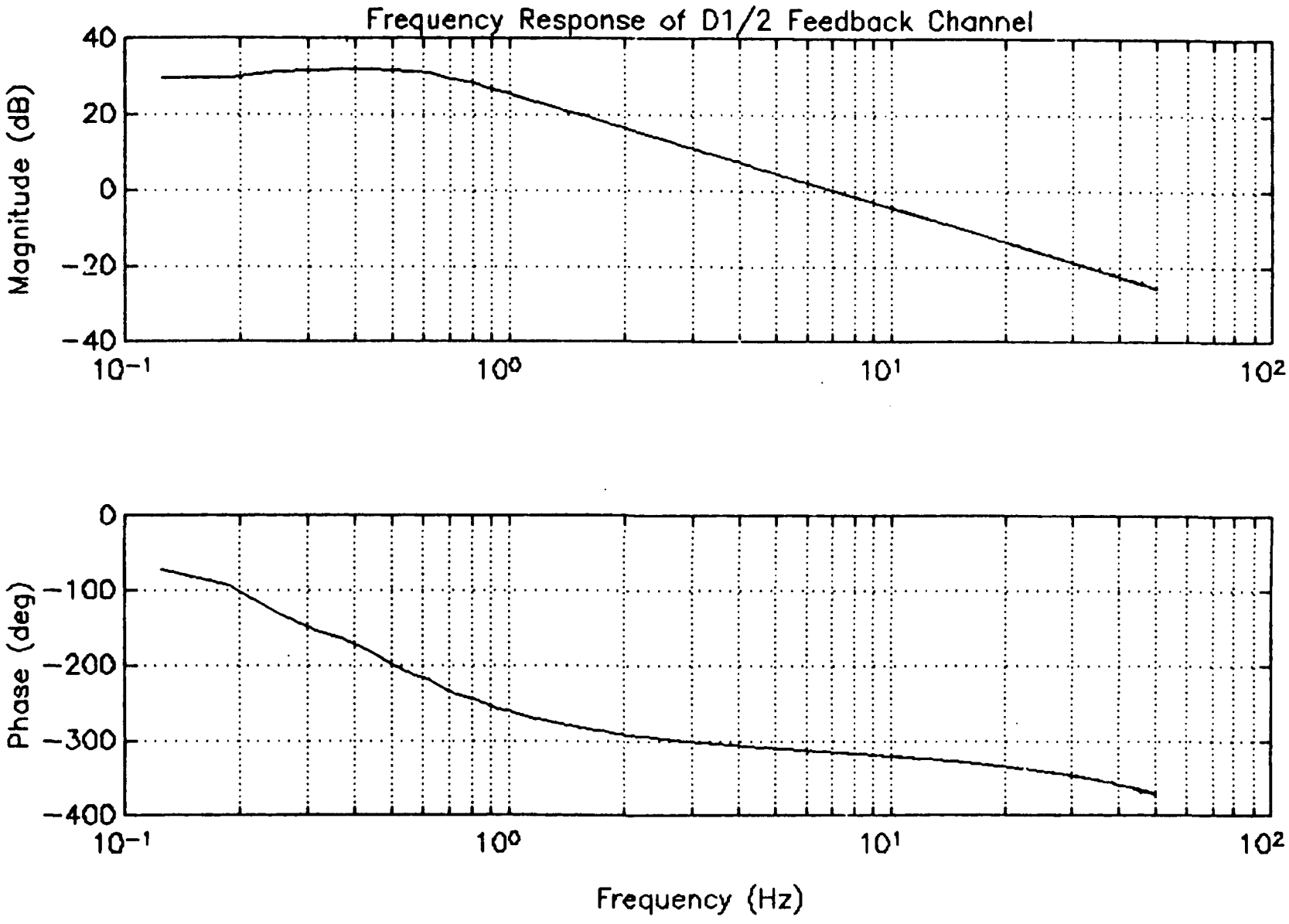

Figure 18. Frequency Response of D $\frac{1}{2}$ Feedback Channel

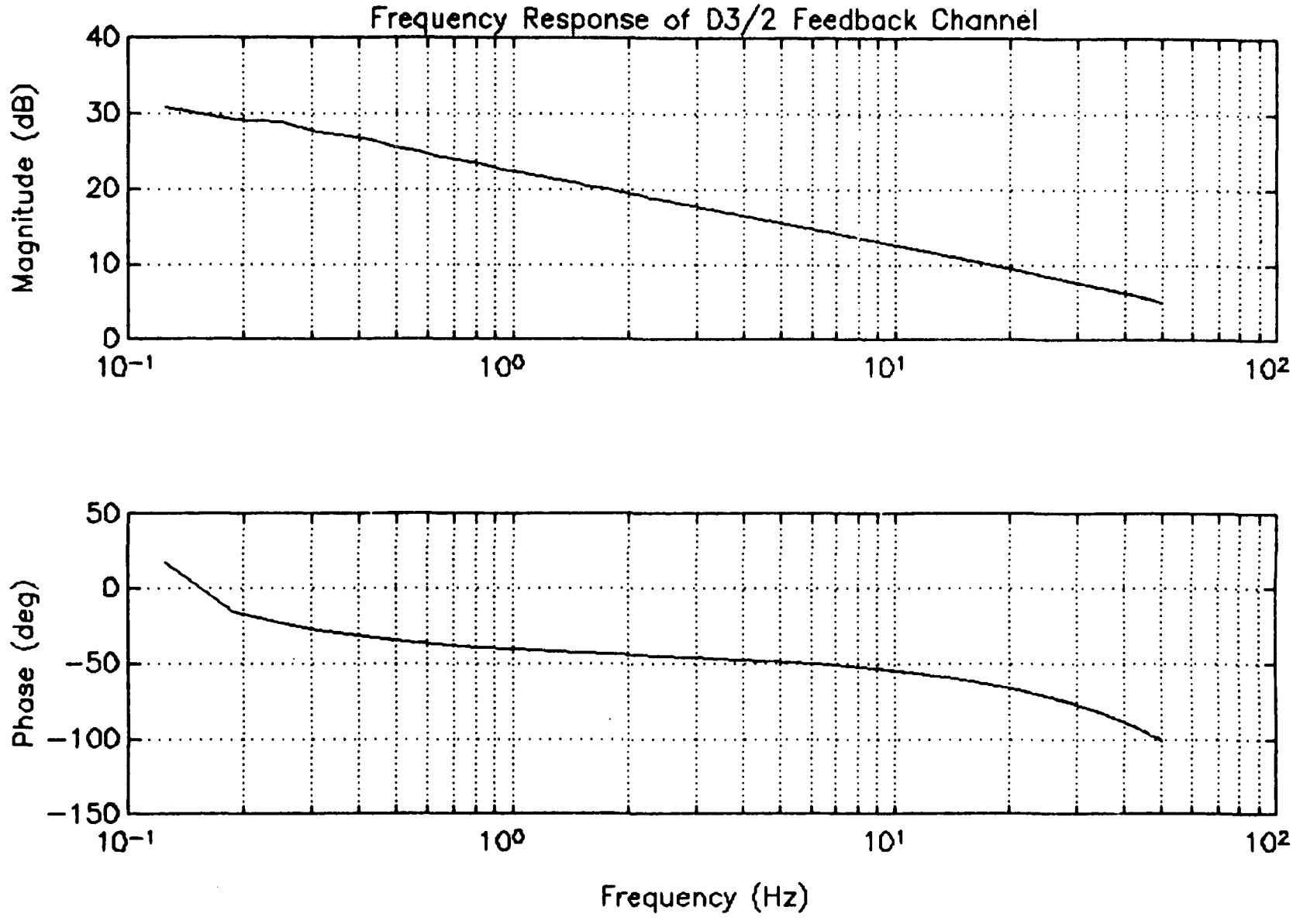

Figure 19. Frequency Response of D $\frac{3}{2}$ Feedback Channel

VI. LQR Control Method

Overview

The original intent of this thesis was to experimentally prove the validity of the work done by Yang(30). He showed that it is theoretically possible to transform the integer-order (position and velocity) controller calculated by the Linear Quadratic Regulator (LQR) problem into an equivalent controller containing the desired fractional order terms. This method was approached using both the 22 degree-of-freedom finite element model and the reduced two degree-of-freedom model.

Review of Optimal Control Theory

A frequently applied form of optimal control theory is the Linear Quadratic Regulator. A regulator is defined as "a feedback controller designed to keep a stationary system within an acceptable deviation from a reference condition using acceptable amounts of control." (9: 167) An LQ regulator provides the optimal solution to a linear system of equations (such as the state space model developed previously) evaluated on a quadratic performance index, J. J is written as

$$J = \int_0^\infty \left[\underline{x}^T(t) \mathbf{Q} \underline{x}(t) + \underline{u}^T(t) \mathbf{R} \underline{u}(t) \right] dt \qquad (43)$$

where **Q** is a positive-semidefinite or positive-definite matrix weighting the states, and **R** is a positive-definite matrix weighting the control input. Because there is only a single actuator, in this problem $\underline{u}(t)$ and **R** are both scalar. For structural dynamics, a convenient choice of **Q** is

$$Q = \begin{bmatrix} k & 0 \\ 0 & m \end{bmatrix} \tag{44}$$

which minimizes the kinetic and potential energy in the beam. **R** is chosen according to how much control authority is available in the actuators and how much control is desired over the structure. When **R** is made smaller, the amount of control force is increased which intuitively seems like it should improve performance. However, this also increases the bandwidth of the controller, which increases the sensitivity of the system to any noise in the measurements or errors in the system model.

The LQ regulator is chosen to minimize this performance index for a particular system. It is calculated from the solution, **S**, of the matrix Riccati equation

$$0 = A^T S + SA - SBR^{-1}B^T S + Q \tag{45}$$

The optimal gain for the LQ regulator is

$$\underline{u} = -R^{-1}B^T S\underline{x} = -G\underline{x} \tag{46}$$

The state model can now be rewritten as

$$\dot{\underline{x}} = \mathbf{A}\underline{x} + \mathbf{B}\underline{u} = [\mathbf{A} - \mathbf{BG}]\underline{x} \tag{47}$$

A caveat is necessary at this point; this solution is optimal only in a mathematical sense and is only as good as the system model and performance index chosen. It will only give what is asked for in the performance index (with respect to a realistic criterion of optimality), and makes no consideration of robustness issues with respect to noisy measurements.

Fractional Order State Feedback Control Theory

Interest in fractional order state feedback control grew from interest in examining the effect of feedback in controlling viscoelastically damped structures. Bagley and Torvik (7) showed that fractional order state equations can be developed where the state vector includes fractional order time derivatives of a structure's motion. The fractional order state equations can be written as

$$D^{\alpha}\,\underline{y} = \mathbf{A}\underline{y} - \mathbf{BG}\underline{y} \tag{48}$$

where $\underline{y}$ is the fractional state vector.

Yang (30) developed a method of calculating meaningful feedback gains for such a fractional order formulation. This section summarizes his work. He

developed a relation, Φ, between the integer order and fractional order state vectors,

$$\underline{x} = \Phi \underline{y} \tag{49}$$

where Φ is a state transformation matrix which can be determined from the eigenstructure of the equations of motion posed in expanded form.

Looking at the N degree-of-freedom vibration problem described described earlier, with damping set to zero,

$$m\ddot{z} + kz = Du \tag{28}$$

and applying the composition property of the fractional derivative operator, Eq (28) can be transformed into

$$\begin{aligned} D^{\alpha} m\left[D^{2-\alpha} + D^{2-2\alpha} + D^{2-3\alpha} + \ldots + D^{0}\right] z(t) \\ - m\left[D^{2-\alpha} + D^{2-2\alpha} + D^{2-3\alpha} + \ldots + D^{\alpha}\right] z(t) \\ + k D^{0} z(t) = Du(t) \end{aligned} \tag{50}$$

This equation represents the same system in (28), but expressed in terms of fractional order derivatives. To ensure that velocity terms appear in the fractional order state equations, α for this problem is chosen to be of the form $\frac{1}{n}$ where n is an integer. This allows initial value problems to be solved where an initial velocity is given.

In order to solve this system of equations, it is possible to expand these N equations into a new system of $2 \cdot N \cdot n$ equations of the form

$$D^{\alpha} \tilde{\mathbf{M}}\, \tilde{\mathbf{z}}(t) + \tilde{\mathbf{K}} \tilde{\mathbf{z}}(t) = \tilde{\mathbf{F}}(t) \tag{51}$$

where

$$\tilde{\mathbf{M}} = \begin{bmatrix} 0 & 0 & \dots & 0 & m \\ 0 & 0 & \dots & m & 0 \\ \vdots & \vdots & \vdots & \vdots & \vdots \\ 0 & m & \dots & 0 & 0 \\ m & 0 & \dots & 0 & 0 \end{bmatrix} \tag{52}$$

$$\tilde{\mathbf{K}} = \begin{bmatrix} 0 & 0 & \dots & 0 & -m & 0 \\ 0 & 0 & \dots & -m & 0 & 0 \\ \vdots & \vdots & \vdots & \vdots & \vdots & \vdots \\ 0 & -m & \dots & 0 & 0 & 0 \\ -m & 0 & \dots & 0 & 0 & 0 \\ 0 & 0 & \dots & 0 & 0 & k \end{bmatrix} \tag{53}$$

$$\tilde{\mathbf{z}}(t) = \begin{Bmatrix} D^{2-\alpha} z(t) \\ D^{2-2\alpha} z(t) \\ \vdots \\ D^{2\alpha} z(t) \\ D^{\alpha} z(t) \\ z(t) \end{Bmatrix} \tag{54}$$

$$\tilde{\mathbf{F}}(t) = \begin{bmatrix} \mathbf{0} \\ \mathbf{0} \\ \vdots \\ \mathbf{0} \\ \mathbf{0} \\ \mathbf{D}\underline{u}(t) \end{bmatrix} \tag{55}$$

This augmented set of $2 \cdot N \cdot n$ equations is called the expanded equations of motion of the system. $\tilde{\mathbf{M}}$ and $\tilde{\mathbf{K}}$ are known as the pseudo-mass and the pseudo-stiffness matrices. Notice that the lowest partition of Eq (51) above identical to the original equation, Eq (28).

Setting the right hand side of Eq (51) equal to zero, it is possible to solve for the resulting homogeneous system's expanded eigenvalues and eigenvectors. The eigenvalues will appear in complex conjugate pairs, λ_i and $\bar{\lambda}_i$. The eigenvectors ($\underline{\Phi}_i$ and $\bar{\underline{\Phi}}_i$ associated with the conjugate eigenvalue pairs) will be used to construct a state transformation matrix to the integer order state equation.

From the expansion theorem of theoretical modal analysis it is known that the system response can be written in terms of the normal modes of the system multiplied by a set of time-dependent generalized coordinates,

$$\underline{q}(t) = \Phi \underline{\eta}(t) \tag{56}$$

where

$\underline{q}(t)$ = column vector of the generalized system response

Φ - the modal matrix consisting of the modal vectors arranged in a matrix

$\underline{\eta}(t)$ - a column vector of the modal coordinates of the system.

Applying this to the expanded equations of motion, it is possible to express the system response as

$$\tilde{z}(t) = \tilde{\Phi}\,\underline{\eta}(t) \tag{57}$$

where

$$\tilde{\Phi} = \left[\, \Phi_1 \mid \bar{\Phi}_1 \mid \Phi_2 \mid \bar{\Phi}_2 \mid \ldots \mid \Phi_N \mid \bar{\Phi}_N \,\right] \tag{58}$$

$$\underline{\eta}(t) = \begin{Bmatrix} \eta_1(t) \\ \bar{\eta}_1(t) \\ \eta_2(t) \\ \bar{\eta}_2(t) \\ \vdots \\ \eta_N(t) \\ \bar{\eta}_N(t) \end{Bmatrix} \tag{59}$$

Using Eq (57) it is possible to extract the necessary information to construct the integer state vector and the fractional state vector for the system. The stable roots of the expanded equations of motion have positive real parts. To begin with select the column vectors (Φ_i) of Eq (58) that

correspond to the eigenvectors in Eq (59) that have positive real components. Define this matrix as $\tilde{\Phi}_p$.

The integer state vector can be written as

$$\underline{x}(t) = \Phi_A \underline{\eta}(t) \tag{60}$$

where $\underline{x}(t)$ is defined as

$$\underline{x}(t) = \begin{Bmatrix} z(t) \\ D^1[z(t)] \end{Bmatrix} \tag{61}$$

and

Φ_A = matrix consisting of row vectors in $\tilde{\Phi}_p$ that are associated with the states defined in Eq (61)

Similarly, the fractional state vector, $\underline{y}$, can be written as

$$\underline{y}(t) = \Phi_B \underline{\eta}(t) \tag{62}$$

where

$$\underline{y}(t) = \begin{Bmatrix} y_1(t) \\ y_2(t) \\ y_3(t) \\ \vdots \\ y_{2N-1}(t) \\ y_{2N}(t) \end{Bmatrix} \tag{63}$$

Φ_B = matrix consisting of row vectors in $\tilde{\Phi}_p$ that are associated with the states defined in Eq (63)

The fractional state vector, $\underline{y}(t)$, is a nearly arbitrary subset of $\tilde{z}$ (t) (the state vector of the expanded equations of motion). It is of the same dimension as the integer state vector, and may contain any combination of fractional and integer order states from any combination of nodes.

From Eq (62) $\underline{\eta}$ may be defined as

$$\underline{\eta}(t) = \Phi_B^{-1}\, \underline{y}(t) \tag{64}$$

Which can be substituted into Eq (60)

$$\underline{x}(t) = \left[\Phi_A \ \Phi_B^{-1}\right] \underline{y}(t) = \Phi\, \underline{y}(t) \tag{65}$$

Which is the desired transformation from integer state vector to fractional state vector.

Applying this result to the integer state optimal control law in Eq (47)

$$\Phi \dot{\underline{y}}(t) - [A - BG] \Phi \underline{y}(t) \tag{66}$$

Which can be rewritten as

$$\dot{\underline{y}}(t) - [A^* - B^*G^*] \underline{y}(t) \tag{67}$$

where

$$A^* - \Phi^{-1} A \Phi \tag{68}$$

$$B^* - \Phi^{-1} B \tag{69}$$

$$G^* - G \Phi \tag{70}$$

This is the desired result of a set of fractional order state equations with optimal LQR feedback control.

Results

There were several problems observed when the LQR method was implemented. The finite element model used was not suitable for use with LQR, and the classical integer order controllers generated with it were not very effective. As mentioned before, the finite element model was only accurate for the first two modes, and had fifty percent error in frequency for

mode three, with higher order modes being progressively more poorly represented. Since LQR weights all modes equally when formulated in position variables, the poor information dominated the correct information for the first two modes. The LQR method did indeed give an optimum solution, but it was for a structure that did not exist. Because of all the control force required to control all twenty-two modes of the model, the actuator reached its force limits before modes one and two had reached even five percent critical damping.

The reduced order, two degree-of-freedom model gave much better performance. The integer order LQR gains were meaningful, and produced the desired damping levels in the structure, but when the fractional order state vector was calculated, the gains on the fractional derivative terms were nearly ignored. For example, solving the LQR problem using PC-Matlab (22) for R = 0.1 yielded integer order gains of

$$\mathbf{G} = \begin{bmatrix} 7.90 & -0.960 & -0.471 & 0.0969 \end{bmatrix} \tag{71}$$

for a state vector composed of

$$\mathbf{x}(t) = \begin{Bmatrix} z(t) \\ D^1[z(t)] \end{Bmatrix} \tag{72}$$

For a state vector composed of

$$\underline{y}(t) = \begin{Bmatrix} D^{\frac{3}{2}}[z_1(t)] \\ D^{1}[z_1(t)] \\ D^{\frac{1}{2}}[z_1(t)] \\ z_1(t) \end{Bmatrix} \tag{73}$$

the state transformation matrix, Φ^*, was calculated to be

$$\Phi^* = \begin{bmatrix} 0 & 0 & 0 & 1 \\ -0.00360 & -0.05351 & 0.331 & 3.50 \\ 0 & 1 & 0 & 0 \\ 0.331 & -10.2 & 115 & -451 \end{bmatrix} \tag{74}$$

Using this transformation a new set of gains is calculated, G^*, is found to be

$$G^* = \begin{bmatrix} 0.0286 & -0.470 & 10.9 & -39.2 \end{bmatrix} \tag{75}$$

Although this result is taken from measurements at only the midpoint, it should theoretically provide the same control authority as the controller using position and velocity measurements from both points.

Another possibility is feeding back the velocity and $D^{\frac{3}{2}}$ terms from both sensors. This would eliminate the need for the second integration process and the consequent phase distortion caused by the high-pass filter. The transformation matrix for this term will be denoted by Φ^* and was found to be equal to

$$\Phi^* = \begin{bmatrix} -0.00166 & -0.000973 & 0.00935 & 0.00380 \\ -0.00530 & -0.00467 & 0.0207 & 0.0211 \\ 0 & 0 & 1 & 0 \\ 0 & 0 & 0 & 1 \end{bmatrix} \tag{76}$$

and the associated gain, G^*, is

$$G^* = \begin{bmatrix} -0.00802 & -0.00321 & 0.525 & 0.107 \end{bmatrix} \tag{77}$$

where the associated state vector is

$$\underline{y}(t) = \begin{Bmatrix} D_2^{\frac{3}{}} [z(t)] \\ D^1 [z(t)] \end{Bmatrix} \tag{78}$$

The numerical results are shown below in Table 3, while the closed loop frequency response is shown in Figure 20.

Table 3. Results of LQR Method (Percentage of Critical Damping)

Mode	Predicted	G	G^*	G^*
1	21.1%	22.3%	18.5%	18.6%
2	10.9%	8.5%	1.8%	7.5%

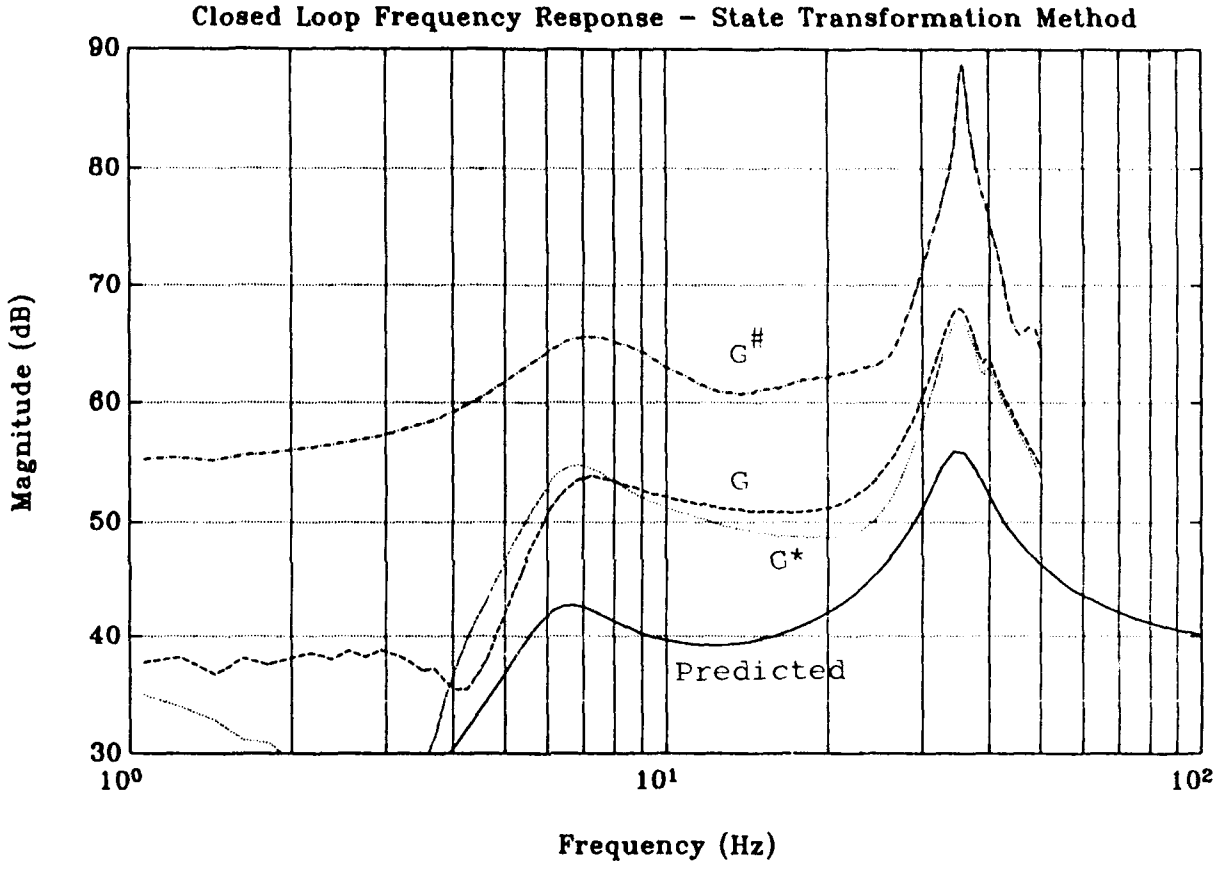

Figure 20. Closed Loop Frequency Response of LQR Method

The results shown are promising but certainly not conclusive. As in the open loop case, there is a large discrepancy between the predicted and measured closed loop response. The shape of the predicted response corresponds well to the experimentally measured ones, but there is a large offset in magnitude that needs to be resolved at some point.

Comparing the integer order case, **G**, to the cases with fractional order feedback ($\mathbf{G}^*$ and $\mathbf{G}^\#$) still yields some useful information, however. The case where all measurements have been taken from a single point (collocated with the actuator), $\mathbf{G}^\#$, is only marginally stable, with audible high frequency resonances occuring. The performance is degraded for the first mode, but still provides a reasonable amount of damping. Performance at the second mode is abysmal, and even destabilizes the system somewhat. (The friction in the armature of the actuator provides 2.2% damping for mode 2 when the actuator is attached but unpowered, so the performance would actually be improved at this frequency by turning the system off.)

The case where signals are taken from both sensors, $\mathbf{G}^*$, is much more promising. The closed loop response is very similar to that of the integer order case, although there is still some degradation in the performance of the system. Because of the known errors in the system (modelling errors and phase shifts in the measurements), it is not possible to say conclusively that fractional order feedback is equivalent to integer order feedback. However, it possible to say that the method of transforming integer order gains into an equivalent system containing mixed fractional and integer order gains does seem to be successful. The fact that control remains stable in the face of such large phase shifts in the measurements even indicates reasonably large phase margins, and some degree of robustness.

VII Pole Placement Control Method

Overview

An alternative approach to introducing fractional order feedback into structural control was discovered by Leonard (15). He found an interesting result that seemed to allow a large amount of flexibility when selecting pole placement gains if fractional order feedback signals were available. The theory presented here summarizes much of Leonard's work. Briefly, it calculates a set of equality and inequality constraints between the fractional and integer order terms that is necessary for equivalent response to be obtained. Once again, the primary goal of this research was proof of concept, showing that fractional derivative feedback would work in a real system.

Theory

Assuming an nth order linear dynamic system of the form

$$\dot{\mathbf{x}}(t) = \mathbf{A}\mathbf{x}(t) + \mathbf{B}\mathbf{u}(t) \tag{79}$$

where $\mathbf{x}$ contains integer order feedback terms (position and velocity) and there exists state feedback

$$\mathbf{u}(t) = -\mathbf{G}\mathbf{x}(t) \tag{80}$$

where

$$G = [g_1 \; g_2 \; \cdots \; g_n] \tag{81}$$

So that the system can be written

$$\underline{\dot{x}}(t) = [A - BG]\underline{x}(t) \tag{82}$$

Let $\alpha(s)$ be an equation with the desired pole structure of the system

$$\alpha(s) = \prod_{1}^{n}(s - p_i) = 0 \tag{83}$$

In order for the gain matrix to move the poles of the system to the desired locations, the characteristic equation of the closed-loop system must equal

$$\det[sI - A + BG] = \alpha(s) = 0 \tag{84}$$

In other words, the coefficients of the characteristic equation must equal the coefficients of $\alpha(s)$.

Now suppose that the equations of the system were posed in fractional state form.

$$D^{\frac{1}{2}}[\underline{x}_F(t)] = A\underline{x}_F(t) + B\underline{u}(t) \tag{85}$$

where $\underline{x}_F(t)$ now includes the half order fractional states

$$\mathbf{x}_F(t) = \begin{Bmatrix} \mathbf{x}(t) \\ D^{\frac{1}{2}}[\mathbf{x}(t)] \\ D^{1}[\mathbf{x}(t)] \\ D^{\frac{3}{2}}[\mathbf{x}(t)] \end{Bmatrix} \tag{86}$$

Examining the pole placement problem in this case requires a little more work. Consider the transformation

$$\beta = \sqrt{s} \tag{87}$$

The eigenvalue problem for the fractional state case is posed as

$$\det\left[\beta\mathbf{I} - \mathbf{A} + \mathbf{BG}\right] = 0 \tag{88}$$

The fractional state system has twice as many poles as the integer state system in the $\sqrt{s}$ or β plane. This function is not unique, and a discontinuity must exist somewhere in the space. Poles in the β plane with phases of greater than 90° or less than -90° cross a branch cut, and will map to another Riemann sheet when they are brought back into the s-plane (See Figure 21). The stability criterion in the β plane is that the phase of a pole must lie in the ranges of

$$45^\circ < \phi < 90^\circ \tag{89}$$

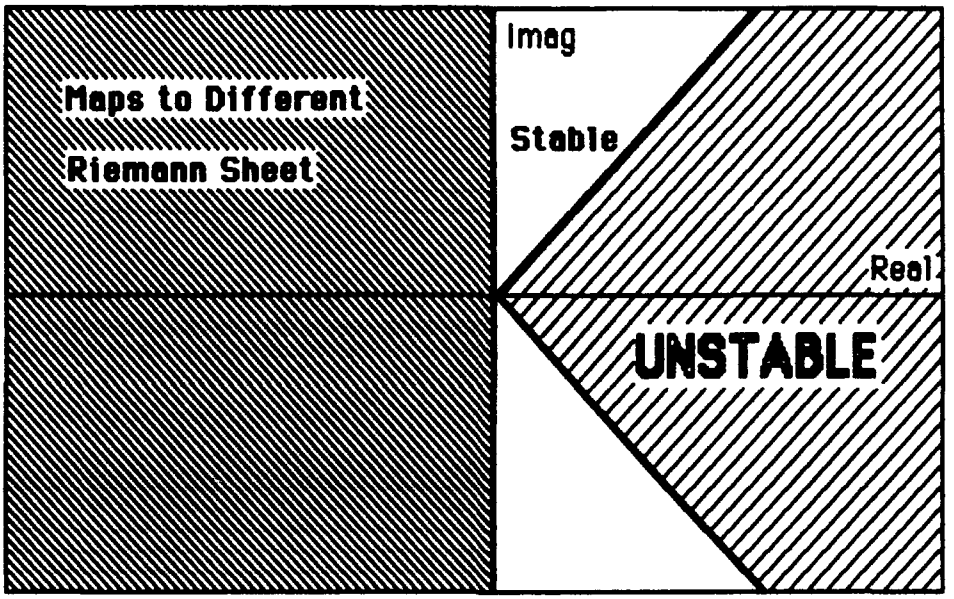

Figure 21. Stability Diagram of β Plane

or

$$-45^\circ > \phi > -90^\circ \quad . \tag{90}$$

So now each real pole, p_i, may be factored into two poles in the β plane. There are n pairs of poles and 2n gains so it appears that the expanded problem has left you in a similar situation to where you began, except that the order of the system has doubled. If this were true, this would be a remarkably useless result; however, it is only necessary to control *half* of these poles. To retain similar control authority to the integer state problem, it is only necessary to place n poles in the right half plane. The other n poles merely need to be kept in the left half β plane off of the principal Riemann sheet to ensure stability.

To take advantage of this, first compute the square roots of the desired pole locations:

$$\hat{p}_i = \sqrt{p_i} \tag{91}$$

Form

$$\Omega(\beta) = \prod_{i=1}^{n}(\beta - \hat{p}_i) \tag{92}$$

Form the characteristic equation of the system in the β plane

$$Z(\beta) = \det\left[\beta \mathbf{I} - \mathbf{A} - \mathbf{BG}\right] = 0 \tag{93}$$

Since Z is of order 2n and Ω is only of order n, synthetic division is possible. Performing synthetic division on $Z(\beta)$ with $\Omega(\beta)$ yields $\Psi(\beta)$ and $R(\beta)$, the remainder.

$$\frac{Z(\beta)}{\Omega(\beta)} = \Psi(\beta) + \frac{R(\beta)}{\Omega(\beta)} \tag{94}$$

$\Psi(\beta)$ is a polynomial of order n. For $\Omega(\beta)$ divide evenly in to $Z(\beta)$, and be equal to its roots, the coefficients of $R(\beta)$ must be equal to zero. This creates n equality constraints on the system.

$\Psi(\beta)$ contains the n poles that are not mapped into the s plane, so they must lie in the left hand β plane. To ensure their stability, it is possible to

use Routh-Hurwitz criterion to create inequality constraints that provide bounds on stability.

The Routh-Hurwitz criterion (18: 363-365) states that for an equation of the form

$$a_0 s^m + a_1 s^{m-1} + a_2 s^{m-2} + \ldots + a_{m-1} s + a_m = 0 \qquad (95)$$

to be stable, all coefficients a_i must be of the same sign and not equal to zero, and, the coefficients of the first column of the Routh array must also have the same sign.

These inequality constraints define a region in the controller space, and any solution lying in this region should provide a stable solution. This means that the problem has an infinite number of non-unique solutions, all of which satisfy stability requirements. From a control system design viewpoint, this is a very interesting result.

At this point, there are no guidelines as to how best use this design flexibility. However, since any set of gains that satisfy these constraints should work, and the object of this thesis was merely to prove that fractional derivative feedback is possible, this method was acceptable, if somewhat awkward.

Results

Because of the synthetic division in this method, there is not yet a constructive solution to this problem. Rather than solving a series of high order determinants and a lengthy synthetic division by hand, the symbolic

capabilities of Mathematica(29) were brought to bear on the problem. The script used to calculate the equality and inequality constraints and the constraints themselves are shown in Appendix G.

Arbitrarily choosing damping ratios of twenty percent for mode 1 and ten percent on mode 2, the desired pole locations were calculated using

$$p_i = \left(-\zeta_i w_i \pm \sqrt{1 - \zeta_i^2}\, w_i \right) \tag{96}$$

Using the system model developed in Eqs (37) and (38) the following integer order gains were calculated from Eq (85)

$$G_p = \begin{bmatrix} -3.16 & 2.34 & 0.566 & 0.115 \end{bmatrix} \tag{97}$$

Using this solution as a starting point, the integer order gains were reduced in magnitude while the four dependent fractional gains were calculated using the equality constraints. The resulting set of gains was checked versus the inequality constraints to ensure that the closed loop system would still be stable. The first controller developed contained all eight feedback states (two each of position, velocity, $D^{\frac{3}{2}}$, and $D^{\frac{1}{2}}$ terms), arranged as in Eq (86).

$$G1 = \begin{bmatrix} 1.5 & -2 & 1.08 & 0.886 & 0.4 & 0.02 & 0.0138 & 0.00743 \end{bmatrix} \tag{98}$$

The second controller was calculated by zeroing the position and $D^{\frac{1}{2}}$ terms, with only velocity and $D^{\frac{3}{2}}$ terms being fed back. The equality constraints provided the necessary information to calculate the other four gains. It was

thought that this might prove to be a useful special case because of the difficulty with performing the second integration discussed in Chapter 3.

$$G2 = \begin{bmatrix} 0.591 & 0.176 & -0.00730 & -0.00776 \end{bmatrix} \quad (99)$$

These three controllers were tested and the resulting closed loop transfer functions plotted versus the theoretical closed loop transfer function for the system in Fiqure 22. The results are listed in Table 4.

Table 4. Results of Pole Placement Method

	Predicted	G_p	G1	G2
Mode 1	20%	21.6%	19.3%	20.1%
Mode 2	10%	10.1%	10.6%	8.6%

The results agree fairly well with the predicted values. The shape of the predicted response again corresponds well to the experimentally measured ones, but there is the same large offset in magnitude as was present in the previous case.

However, the most important comparison to be made here is that between the integer order controller, G_p, and the controllers using fractional states, G1 and G2. The point of this work was to show that control using fractional order feedback was equivalent to schemes using the more thoroughly studied integer order feedback. Since these controllers were

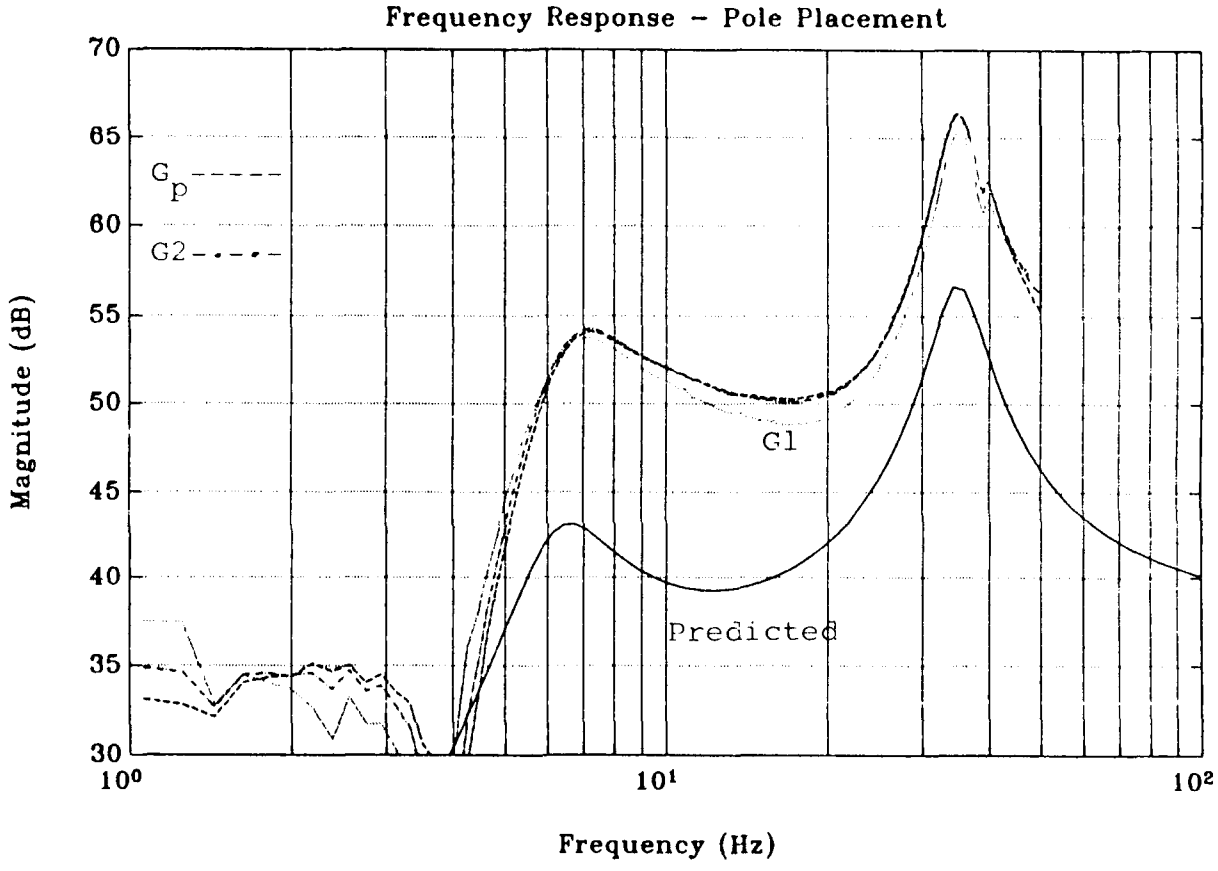

Figure 22. Closed Loop Frequency Response of Pole Placement Method

calculated from the same model, whatever its inaccuracies, the results should be very similar. These numbers show that this is indeed true.

Comparing the integer order feedback, G_p, to the **G1** and **G2** controllers, **G1** displays an error of 11% and 5% for modes one and two respectively, while **G2** shows an error of 6.9% and 15% respectively. These results are encouraging, particularly in light of the known errors in the circuitry. Because of the large phase shifts present in the fractional derivative feedback due to the final low pass filtering process, it was anticipated that some loss of control authority would occur. In fact, it is encouraging that these controllers are robust enough to still produce stable control in the presence of such a large phase lag.

A final result is the force history in the time domain of the system with the various controllers in the loop. It was a prior concern that there might be some undesirable transients in the force response because of the effects of the poles off of the principal Riemann sheet. Those poles that are close to the branch cut can "bleed over" and influence the system behavior. However, those worries seem to be unfounded, and the force histories of the different controllers are qualitatively similar. They are shown in Figure 23.

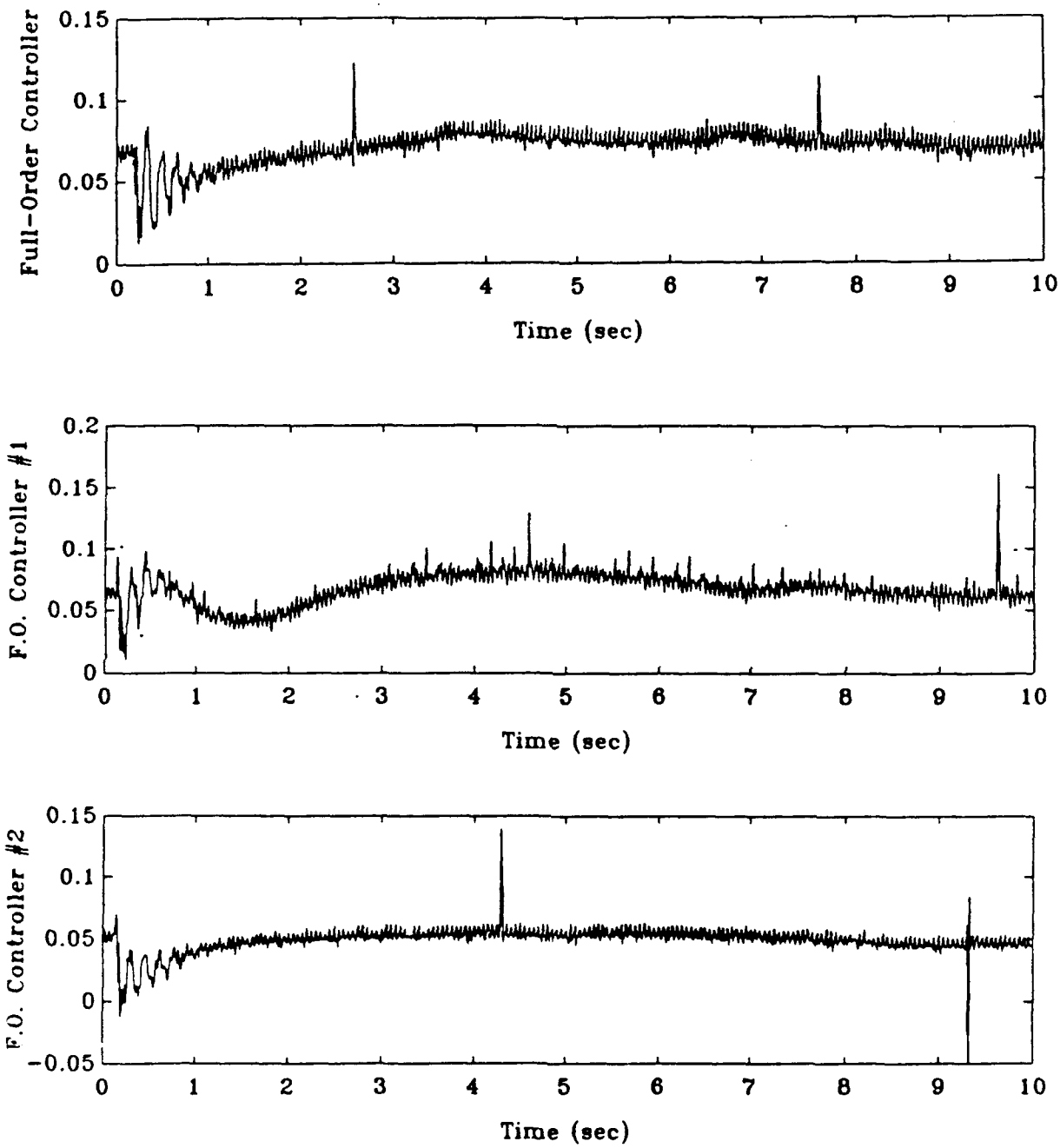

Figure 23. Experimental Force Histories

Comparison of the Two Methods

Because of the equality constraints of the pole placement method, any case with just four non-zero gains should be unique (if a solution exists), since the problem reduces to four linear equations in four unknowns. If that is so, the question is, is there any correspondence between results calculated by the LQR method and the pole placement method? In this chapter, gains were calculated for both the integer order case (position and velocity only) and the case where velocity and the $D^{\frac{3}{2}}$ signals were fed back from both sensors. In the last chapter, a relationship between those two gains was calculated in Eq (76), so it is possible to compare the two results.

Using the results of Eq (97) and Eq (76),

$$G_{ST} = G_p \Phi^* = \begin{bmatrix} 0.585 & 0.152 & -0.00715 & -0.00784 \end{bmatrix} \qquad (100)$$

which compares well with the result from Eq (99)

$$G2 = \begin{bmatrix} 0.591 & 0.176 & -0.00730 & -0.00776 \end{bmatrix} \qquad (101)$$

Since the pole placement method keeps track of the poles that lie off of the principal Riemann sheet, it is probably the more accurate of the two techniques. Additionally, it is the more general of the two techniques, since it allows all $2 \cdot n$ gains to be assigned while the state transformation technique of the last chapter only allows the use of a subset containing n of the gains.

VIII. Conclusions and Recommendations

The theoretical predictions made by Yang (30) and Leonard (15) both performed as expected within the bounds of the experiment's error. Fractional derivative feedback may in fact prove workable in a real world setting in the future. Based on the results of this work, it at least merits further consideration and research.

There are several topics that need to be addressed before any more positive recommendations can be made. The first is, what can fractional derivative feedback accomplish that integer order feedback cannot? Feeding back twice as many inputs to get the same control authority is not an idea that is going to be of much use to designers. On the other hand, if those extra inputs can be used to improve system performance, particularly to increase system robustness, it becomes more attractive and potentially useful.

Second, developing a mass-stiffness model for a real structure is somewhat unwieldy, a modal model is in general easier to generate. To do this, a modal estimator for fractional derivatives needs to be developed. Eventually a stochastic estimator (a Kalman filter) would be desirable to have available. Accelerometers tend to be accurate but not precise, and if the measurement noise statistics are available, a Kalman filter can greatly improve system performance. Also, since modeling large space structures in a gravity field is so difficult, building adaptive abilities into a control system is frequently desirable, and many adaptive control systems begin with the Kalman filter as a building block.

The next step for this particular laboratory setup should be the construction or purchase of better filters for the fractional derivative channels. The phase shifts on those channels are unacceptably large, and may well be degrading the performance of the controllers using fractional derivative feedback. Theoretically four fractional derivative feedbacks should provide the same damping as four position and velocity feedbacks do. Currently they do not, there is some degradation of the performance. It should be established whether or not this is the nature of the fractional derivative feedback, or is merely the result of poor filters.

Of equal or greater importance is the resolution of the errors in modeling this system. The unmodelled dynamics are significant in the bandwidth of the system, and a higher order model should be examined. Once the a better model is in hand, this work needs to be repeated, particularly the case where all feedback signals are generated from a signal colocated sensor at the actuator. This is potentially the most useful case and it needs to be conclusively established whether the fractional order feedback is effective.

The pole placement technique used in Chapter 7 is not a design method per se, and it becomes very complex computationally as system order increases. Performing the synthetic division while carrying 2·n gain variables requires a program capable of symbolic mathematical operations (such as Mathematica or MACSYMA) for n greater than four. If it is to be used on more complex systems, a better method needs to be found of calculating the controller gains. Algorithms exist that constructively find the solution to the integer order pole placement problem, and they should be examined to see if an extension to the fractional order case is possible.

Bibliography

1. Acoustic Power Systems, Inc. *Instruction Manual– Electro-Seis Model 113-LA Shaker.* Carlsbad, California, 1989.

2. Acoustic Power Systems, Inc. *Instruction Manual– Dual-Mode Model 114 Amplifier.* Carlsbad, California, 1989.

3. Bagley, R. L. *Applications of Generalized Derivatives to Viscoelasticity.* Ph.D. Dissertation, AFIT/DS/AA/79S-2. School of Engineering, Air Force Institute of Technology (AU), Wright-Patterson AFB OH, Sept. 1979. (Also published as Air Force Materials Laboratory TR-79-4103, Nov. 1979)

4. Bagley, R. L. and R. A. Calico. "The Fractional Order State Equations for the Control of Viscoelastically Damped Structures," *Proceedings of the 30th AIAA Structures, Structural Dynamics, and Materials Conference*, AIAA 89-1213, April, 1989, pp. 487-496.

5. Bagley, R.L. and Peter J. Torvik. "A Theoretical Basis for the Application of Fractional Calculus to Viscoelasticity," *Journal of Rheology* 27: 201-210 (May 1983).

6. Bagley, R.L. and Peter J. Torvik. "Fractional Calculus - A Different Approach to the Analysis of Viscoelastically Damped Structures," *AIAA Journal* 21: 741-748 (May 1983).

7. Bagley, R.L. and Peter J. Torvik. "Fractional Calculus in the Transient Analysis of Viscoelastically Damped Structures," *AIAA Journal* 23: 918-925 (May 1985).

8. Balas, Mark. "Trends in Large Space Structure Control Theory, Fondest Hopes, Wildest Dreams," *IEEE Transactions on Automatic Control*, AC-27: 522-535 (March 1982).

9. Bryson, Arthur E., Jr. and Yu-Chi Ho. *Applied Optimal Control* (Revised Edition). New York: Hemisphere Publishing Corporation, 1975.

10. Endevco Corporation. *Model 2262 Piezoresistive Accelerometer Instruction Manual.* San Juan Capistrano, California, 1989.

11. Endevco Corporation. *Models 4422 and 4423 Signal Conditioners Instruction Manual* San Juan Capistrano, California, 1989.

12. Inman, Daniel J. *Vibration: With Control, Measurement, and Stability.* Englewood Cliffs, New Jersey: Prentice Hall, 1989.

13. Jacques, Capt David R. *Baseline Experiment for Active Control of Structural Vibrations*. MS Thesis, AFIT/GAE/ENY/89D-15. School of Engineering, Air Force Institute of Technology (AU), Wright-Patterson AFB OH, December 1989.

14. Klonoski, Capt Kevin D. *Fractional-Order Feedback in Linear Systems* MS Thesis, AFIT/GA/ENY/88D-05. School of Engineering, Air Force Institute of Technology (AU), Wright-Patterson AFB OH, March 1989.

15. Leonard, Mark. Personal Correspondence. Air Force Institute of Technology, Wright-Patterson AFB OH, 24 May 1991.

16. Meirovitch, Leonard M. *Elements of Vibration Analysis.* (Third Edition) New York: McGraw-Hill Book Company, 1986.

17. Nurre, G.S. et al. "Dynamics and Control of Large Flexible Structures," Journal of Guidance, Control and Dynamics, 7: 514-526 (Sept 1984).

18. Ogata, Katsuhiko. *Modern Control Engineering.* Englewood Cliffs, New Jersey: Prentice-Hall, Inc., 1970.

19 Oldfield, M.L.G. et al. "Design of Wide Bandwidth Analogue Circuits for Heat Transfer Instrumentation in Transient Wind Tunnels," *16th Symposium of the International Centre for Heat and Mass Transfer (Heat and Mass Transfer in Rotating Machinery)* Dubrovnik, D.E. Metzger, Ed., New York: Hemisphere Publishing Corp., 1984.

20. Oldham, K. B. and J. Spanier. *The Fractional Calculus.* Orlando: Academic Press, 1974.

21. Oldham, Keith B. and Cynthia Zoski. "Analogue Instrumentation for Processing Polarographic Data," *Journal of Electroanalytical Chemistry*, 157: 27–51 (January 1983).

22. *PC-Matlab*, Sherborn, MA: The Mathworks, Inc.,1987.

23. Ross, Bertram. "Fractional Calculus," *Mathematics Magazine*, 50: 115-122 (May 1977).

24. Savant, C.J. et al. *Electronic Circuit Design: An Engineering Approach*. Menlo Park, California: The Benjamin/Cummings Publishing Co.,1987.

25. Skaar, Steven B., et al. "Stability of Viscoelastic Control Systems," *IEEE Transactions on Automatic Control*, 33: 348-357 (April 1988).

26. Smith, Ralph J. *Circuits, Devices, and Systems*(Fifth edition).New York: John Wiley and Sons, Inc., 1984.

27. Systolic Systems, Inc. *PC-1000 Systolic Array Processor Operations Manual* Campbell, California, 1984.

28. Torvik, P.J. and R.L. Bagley. "On the Appearance of the Fractional Derivative in the Behavior of Real Materials," Journal of Applied Mechanics, 51: 294-298 (Feb 1984).

29. Wolfram, Stephen. *Mathematica: A System for Doing Mathematics by Computer*. Redwood City, California: Addison-Wesley Publishing Co., 1988.

30. Yang, Capt David L. *Fractional State Feedback Control of Undamped and Viscoelastically-Damped Structures*. MS Thesis, AFIT/GA/ENY/90M-3. School of Engineering, Air Force Institute of Technology (AU), Wright-Patterson AFB OH, March 1990.

Appendix A: Oldham-Zoski Circuit Design

The construction of the Oldham-Zoski circuit closely follows that of the author's in their paper(21). The design values are those given for the $\nu = \frac{1}{2}$ design. For more discussion of this design, see also (14). Table A.1 lists the design and experimental values for the test circuit built.

Table A.1 Design and Experimental Values of Oldham-Zoski Components

	Resistors (in MΩ)			Capacitors (in μF)	
Resistor	Design	Measured	Capacitor	Design	Measured
R_0	25.4	25.4	C_0	10.0	10.03
R_1	9.88	9.86	C_1	3.891	3.89
R_2	3.84	3.83	C_2	1.514	1.511
R_3	1.501	1.494	C_3	0.589	0.587
R_4	0.5816	0.5821	C_4	0.2292	0.2297
R_5	0.2262	0.2265	C_5	0.0892	0.0876
R_6	0.08798	0.08792	C_6	0.0347	0.0351
R_7	0.00172	0.00172	C_7	0.0270	0.02707
R_8	0.00364	0.00364			

Appendix B: Oldfield-Burd-Doe Circuit Design

The OBD circuit was designed with a series of six resistors and capacitors for this experiment. The capacitances are measured and then suitable resistances are calculated, so their are no design values for the capacitors per se. Again, this is a straightforward application of the method put forth in (19). Design and experimental values are shown in Table B.1.

Table B.1. Design and Experimental Values of OBD Circuit Components

	Resistors (in kΩ)			Capacitors(μF)
	Design	Measured		Measured
R_1	3.695	3.711	C_1	0.0997
R_2	14.00	14.00	C_2	0.2262
R_3	30.64	30.58	C_3	0.475
R_4	64.79	64.79	C_4	1.012
R_5	142.4	142.1	C_5	2.296
R_6	305.3	306.1	C_6	4.655

Appendix C: Chebyshev High-Pass Filter Design

The high-pass filters that were eventually built for this experiment were the product of as much trial and error as actual design. Active electronic components (such as op-amps) do not function well at extremely low frequencies, and their performance becomes erratic. The filter that provided the best performance when actually built, was a second order Chebyshev filter as shown in Figure 9. The operational amplifier used was an LM-747j, which is a general purpose dual op-amp. The component values that were found to work best were:

C = 0.40 μF

R1 = 447.6 kΩ

R2 = 1.172 MΩ

Appendix D: Butterworth Low-Pass Filter Design

In order to eliminate the resonances caused by high frequency noise entering the sampling process of the A-D board on the PC-1000 in the fractional derivative feedback, it was necessary to construct four Butterworth low-pass filters for the experiment. The circuit diagram is shown in Figure D.1. Once again, LM-747j operational amplifiers were used, and the component values were:

R = 11.8 kΩ

C1 = 190 nF

C2 = 95 nF

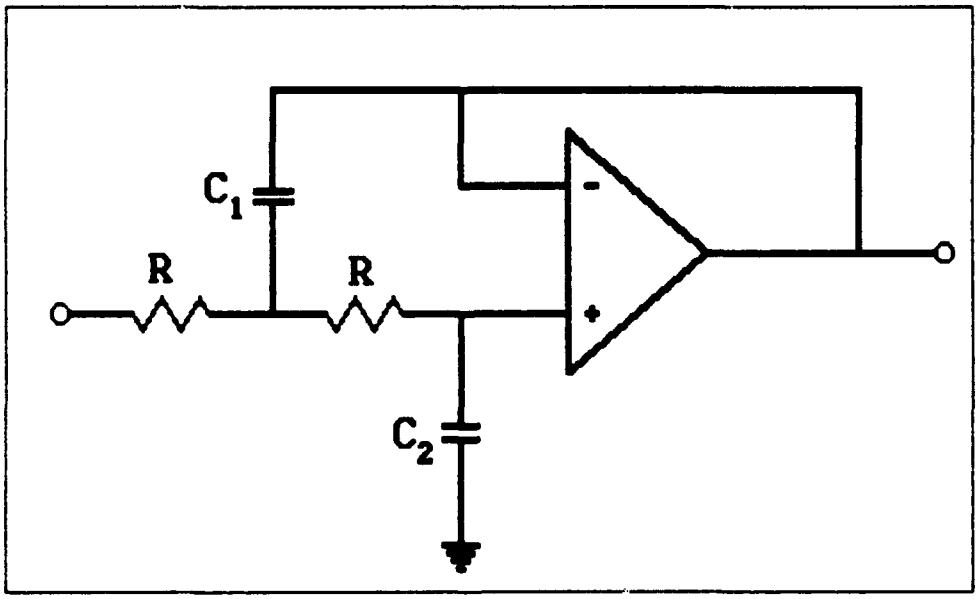

Figure D.1 Circuit Diagram of Butterworth Low-Pass Filter

Appendix E: Finite-Element Model

The finite-element model for this structure is drawn directly from Yang (30:77-78) and models the beam as an undamped 22 degree-of-freedom system. It models the beam's behavior by looking at lateral motion and rotation at eleven points. It also assumes that both lateral bending in the other direction and torsional motion are completely uncoupled from bending in the z direction. The mass and stiffness matrices are constructed from elemental matrices, $\mathbf{K}_{el}$ and $\mathbf{M}_{el}$, which are given by

$$\mathbf{K}_{el} = \frac{EI}{L_e^3}\begin{bmatrix} 12 & 6L_e & -12L_e & 6L_e \\ 6L_e & 4L_e^2 & -6L_e & 2L_e^2 \\ -12L_e & -6L_e & 12 & -6L_e \\ 6L_e & 2L_e^2 & -6L_e & 4L_e^2 \end{bmatrix} \tag{F.1}$$

and

$$\mathbf{M}_{el} = \frac{\rho A L_e}{420}\begin{bmatrix} 156 & 22L_e & 54 & -13L_e \\ 22L_e & 4L_e^2 & 13L_e & -3L_e^2 \\ 54 & 13L_e & 156 & -22L_e \\ -13L_e & -3L_e^2 & -22L_e & 4L_e^2 \end{bmatrix} \tag{F.2}$$

where E, I, ρ, and A are given in Table 1. and L_e is the length of the beam element and is equal to 7.075 in. These elements are summed along the main diagonal to form the 22 DOF mass and stiffness matrices. The mass matrix is further modified to include the mass of the accelerometers at positions x_5

and x_{11} (0.0000343 lb sec^2 in^{-1}) and the mass of the shaker armature at position x_5 (0.00185 lb sec^2 in^{-1}). The model is tuned to match the experimentally determined natural frequencies of the structure by iteratively changing the linear and torsional spring elements connecting the structure to its support.

Appendix F: Experimental Modal Analysis

The modal data of the structure was obtained by performing an experimental modal analysis using a calibrated impact hammer. The procedure has three major steps: Calibration, Data Acquisition, and Data Analysis. The resulting data was used to construct the model of the system, which in turn was used to calculate the controller gains.

Calibration

Two types of sensors are used to acquire data for this test, accelerometers and a force gauge. The accelerometers used are of the piezoresistive type, and can be calibrated versus local gravity by nulling the sensor when its placed in a vertical orientation, then turning it 180° and measuring the resulting voltage. The voltage is proportional to a 2g acceleration and a calibration constant may thus be calculated. Results are shown in Table G.1. These numbers are compared to the manufacturer's specifications as a reality check.

Table G.1. Accelerometer Calibration Data

Accel. Position	Accel. Serial #	Signal Conditioner Gain	2g Meas. (V)	Exp. Cal. Constant (V/g)	Spec. Cal. Constant (V/g)
x_5	AH72	50	1.764	0.882	0.8865
x_{11}	BA26	50	1.996	0.998	0.9915

These numbers compare well, with both being less than one percent off of manufacturer's specifications. For this problem, acceleration is being expressed in $\left(\frac{in}{s^2}\right)$ so these constants are converted to those units. These are sown in Table G.2.

Table G.2. Final Accelerometer Calibration Constants

Accelerometer Serial #	Calibration Constant ($mV/in/s^2$)
AH 72	2.28
BA 26	2.58

The calibration procedure for the force gauge used is somewhat more complex, although the idea behind it is very simple. The problem is only complicated slightly because it is necessary to test the force gauge as it is to be used on the impact hammer. There are two major reasons why this must be so:

1) The impact hammer has a soft tip attached in order to better excite the low frequency modes that are of interest. This soft tip has nonlinear characteristics that must be accounted for that are difficult to predict analytically.

2) The impact hammer behaves differently depending on the way different users strike the test specimen with it. This is due to factors such as the length and mass of the user's arm, among other things.

To calibrate the force gauge, an accelerometer is attached to a small object of known mass, suspended as a pendulum. The accelerometer is mounted on one side of the mass so that its sensitive axis is aligned with the pendular motion. The mass is struck on the other side with the impact hammer, and a transfer function of acceleration to force, $H(s) = \frac{\ddot{z}(s)}{F(s)}$, is computed. From Newton's Second Law it known that this quantity should equal the reciprocal of the known mass (including the mass of the accelerometer). If the same force gauge and accelerometer are to be used to perform the experimental modal analysis, they may be calibrated simultaneously this way with a single calibration constant calculated for the problem. For this test, all measurements will be made relative to the AH72 accelerometer, so the force gauge will be calibrated with respect to that.

The response varies slightly with frequency, and an average value is calculated for the frequency range of interest. The final values are shown in Table G.3.

Table G.3. Calibration Constant for Force Gauge

$\frac{1}{m}\left(\frac{s^2}{lb\text{-}in}\right)$	H(s) (V/in/s²)	Calibration Constant (V/lb)
0.002425	114.6	0.278

Data Acquisition

Now that the system is calibrated it is possible to measure transfer functions for several points along the beam. After acquiring the data on the B&K 2032, it is transfered to the StarModal package for further processing. This package curve fits the data and estimates the modal parameters of each measurement. All measurements are taken with the actuator attached but unpowered. All measurements are taken by striking the impact hammer at the point where the actuator is attached, x_5. The results of this for measurements taken at the two points of interest are shown in Table G.4.

Table G.4. Modal Data From Experimental Measurements

Meas. Pt	x5	x5	x11	x11
Mode	1	2	1	2
Magnitude	3.98	121.9	18.95	144.83
Phase (Deg)	19.1	0.363	0.597	190.6
Damping (%)	6.44	2.04	6.66	2.03
f_n (Hz)	6.24	34.7	6.25	34.7

Data Analysis

The final task remaining is to extract the mode shapes from the modal data found above. The mode shapes are related to modal data by the following relation (12: 195-198),

$$| \underline{s}_r \underline{s}_r^T |_{jk} = | G_{jk}(i \omega_r) | 2^* \zeta_r \qquad (G.1)$$

where

$\underline{s}_r$ is the rth mode shape of the structure

ω_r is the natural frequency of the rth mode

ζ_r is the damping coefficient of the rth mode

G_{jk} is the magnitude of the transfer function at ω_r, measured at point k, and excited at point j (sign is determined from phase information)

The resulting normalized mode shapes are

$$\underline{s}_1 = \begin{bmatrix} 0.203 \\ 1 \end{bmatrix} \qquad \underline{s}_2 = \begin{bmatrix} -0.839 \\ 1 \end{bmatrix}$$

As a check on the reasonableness of this result, these numbers compare favorably with those found from the 22 DOF finite-element model.

$$\underline{s}_1^f = \begin{bmatrix} 0.233 \\ 1 \end{bmatrix} \qquad \underline{s}_2^f = \begin{bmatrix} -0.676 \\ 1 \end{bmatrix}$$

Appendix G: Mathematica Script

```
Gain[a_,b_]:=
Block[{shat,rc,rc1,rp1,rp2},
afem={{0,0,1,0,0,0,0,0},{0,0,0,1,0,0,0,0},
{0,0,0,0,1,0,0,0},{0,0,0,0,0,1,0,0},{0,0,0,0,0,0,1,0},{0,0,0,0,0,0,0,1},{-37268,
{4483.2,-11815,0,0,0,0,0,0}};
bfem={0,0,0,0,0,0,124.6,-93.041};
k={k1,k2,k3,k4,k5,k6,k7,k8};
wn={40.046,218.73};
poles= {(-a+Sqrt[1-a a] I)*wn[[1]],
        (-a-Sqrt[1-a a] I)*wn[[1]],
        (-b+Sqrt[1-b b] I)*wn[[2]],
        (-b-Sqrt[1-b b] I)*wn[[2]]};
shat=poles^.5;
omega=(beta-shat[[1]]) (beta-shat[[2]]) (beta-shat[[3]]) (beta-shat[[4]]);
alpha=Det[beta IdentityMatrix[8]-afem+Outer[Times,bfem,k]];
alpha=Collect[alpha,beta];
omega=Collect[omega,beta];
quot=PolynomialQuotient[alpha,omega,beta];
quot=Collect[quot,beta];
rem=PolynomialRemainder[alpha,omega,beta];
rem=Collect[rem,beta];
rc=CoefficientList[quot,beta];
rp1=rc[[4]] rc[[3]]-rc[[5]] rc[[2]];
rp2=rp1 (rc[[2]]-rc[[4]] rc[[1]]);
rc1=Append[rc,rp1];
rc2=Append[rc1,rp2];
remout=CoefficientList[rem,beta];
equal=Solve[{remout=={0,0,0,0}},{k3,k4,k7,k8}];
equality=Simplify[equal];
equal2=Solve[{remout=={0,0,0,0}},{k5,k6,k7,k8}];
equality2=Simplify[equal2];
ared={{0,0,1,0},{0,0,0,1},{-37268,8235.8,0,0},{44832,-11815,0,0}};
bred={0,0,121.61,-79.026};
kred={K1,K2,K3,K4};
roots=Det[s IdentityMatrix[4]-ared+Outer[Times,bred,kred]];
sroots=Simplify[roots];
listroots=CoefficientList[sroots,s];
Expoles=(s-poles[[1]]) (s-poles[[2]]) (s-poles[[3]]) (s-poles[[4]]);
ExpPoles=CoefficientList[Expoles,s];
Solution=Solve[{listroots==ExpPoles},{K1,K2,K3,K4}]]
```

REPORT DOCUMENTATION PAGE

Form Approved
OMB No. 0704-0188

1. AGENCY USE ONLY *(Leave blank)*	2. REPORT DATE	3. REPORT TYPE AND DATES COVERED
	March 1992	Master's Thesis

4. TITLE AND SUBTITLE
Experimental Feedback of Fractional Order States of a Lightly Damped Structure

5. FUNDING NUMBERS

6. AUTHOR(S)
Robert C. McCall

7. PERFORMING ORGANIZATION NAME(S) AND ADDRESS(ES)
Air Force Institute of Technology, WPAFB OH 45433-6583

8. PERFORMING ORGANIZATION REPORT NUMBER
AFIT/GA/ENY/92M-01

9. SPONSORING/MONITORING AGENCY NAME(S) AND ADDRESS(ES)
Robert Gordon
WL/FIBG
Wright-Patterson AFB, OH 45433

10. SPONSORING/MONITORING AGENCY REPORT NUMBER

11. SUPPLEMENTARY NOTES

12a. DISTRIBUTION/AVAILABILITY STATEMENT
Approved for public release; distribution unlimited

12b. DISTRIBUTION CODE

13. ABSTRACT *(Maximum 200 words)*

The purpose of this study was to investigate the effectiveness of using fractional order time derivatives of position feedback signals in the active control of vibration. To that end, circuitry was built and evaluated that finds the half order time derivative of an input signal. The magnitude response of the fractional derivative circuits is very good, but there are large phase shifts present that may degrade the performance of the controllers. Two methods of incorporating the fractional derivative signals into the controller were examined. One method involved developing a similarity transformation that transforms an integer order state controller into an equivalent controller using fractional or mixed fractional and integer order signals. The second method was a form of traditional pole placement techniques that allowed the direct design of a controller using fractional and integer order feedback signals. Designs were tested on an inverted cantilever beam with control provided by a shaker, and compared to theoretical predictions and to traditional integer order controllers. There is a discrepancy in the modeling that manifests itself as a large offset in magnitude, particularly at very low frequencies. However, controllers utilizing fractional order feedback provided nearly identical control authority to the traditional integer order designs.

14. SUBJECT TERMS
vibration, active control, fractional calculus, feedback control, structural damping

15. NUMBER OF PAGES
100

16. PRICE CODE

17. SECURITY CLASSIFICATION OF REPORT	18. SECURITY CLASSIFICATION OF THIS PAGE	19. SECURITY CLASSIFICATION OF ABSTRACT	20. LIMITATION OF ABSTRACT
Unclassified	Unclassified	Unclassified	UL